Progress in Oceanography 185 (2020) 102319

Contents lists available at ScienceDirect

Progress in Oceanography

journal homepage: www.elsevier.com/locate/pocean

Effect of terrestrial organic matter on ocean acidification and CO_2 flux in an Arctic shelf sea

David W. Capelle[a,*], Zou Zou A. Kuzyk[a], Tim Papakyriakou[a], Céline Guéguen[b], Lisa A. Miller[a,c], Robie W. Macdonald[a,c]

[a] Centre for Earth Observation Science, University of Manitoba, Winnipeg, Manitoba, Canada
[b] Department of Chemistry, Université de Sherbrooke, Sherbrooke, Québec, Canada
[c] Institute of Ocean Sciences, Fisheries and Oceans Canada, Sidney, British Columbia, Canada

ARTICLE INFO

Keywords:
Aragonite
Carbon-cycle
Carbon-dioxide
Arctic
Ocean acidification

ABSTRACT

Recent research has focused on the changing ability of oceans to absorb atmospheric CO_2 and the consequences for ocean acidification, with Arctic shelf seas being among the most sensitive regions. Hudson Bay is a large shelf sea in northern Canada whose location at the margin of the cryosphere places it in the vanguard of global climate change. Here, we develop a four-compartment box-model and carbon budget using published and recently collected measurements to estimate carbon inputs, transformations, and losses within Hudson Bay. We estimate the annual effects of terrestrial carbon remineralization on aragonite saturation (Ω_{Ar}, a proxy for ocean acidification) and on the partial pressure of CO_2 (pCO_2, a proxy for air-sea CO_2 flux) within each compartment, as well as the effects of marine primary production, marine organic carbon remineralization, and terrestrial calcium carbonate dissolution. We find that the remineralization of terrestrial dissolved organic carbon is the main driver of CO_2 accumulation and aragonite under-saturation in coastal surface waters, but this is largely offset by marine primary production. Below the surface mixed layer, marine organic carbon remineralization is the largest contributor to CO_2 accumulation and aragonite under-saturation, and is partially offset by terrestrial $CaCO_3$ dissolution. Overall, the annual delivery and processing of carbon reduces Ω_{Ar} of water flowing through HB by up to 0.17 units and raises pCO_2 by up to 165 μatm. The similarities between Hudson Bay and other Arctic shelf seas suggest these areas are also significantly influenced by terrestrial carbon inputs and transformation.

1. Introduction

Oceans have slowed the accumulation of CO_2 in the atmosphere by absorbing an estimated 30% of the total anthropogenic CO_2 emissions since 1750 (Ciais et al., 2013). However, dissolved CO_2 forms a weak acid in oceans (carbonic acid or H_2CO_3) leading to "the other CO_2 problem", ocean acidification (OA; Doney et al., 2009). The CO_2 added to the ocean has already caused a 30% increase in surface ocean acidity (0.1 drop in pH; Caldeira and Wickett, 2003), which can be sufficient to stress calcium carbonate ($CaCO_3$) shell-producing organisms (Azevedo et al., 2015), alter the speciation of trace metals, and influence the rates of important metabolic reactions (AMAP, 2013; CliC/AMAP/IASC, 2016). Ocean acidification has significant consequences for microbial abundance, marine food webs, ecosystem productivity, and commercial fisheries.

Individual ocean basins display large differences in their ability to absorb atmospheric CO_2 and in their vulnerability to OA. Freshwater dominated, high latitude, northern shelf seas are relatively prone to OA and CO_2 outgassing (AMAP, 2017; Granskog et al., 2009; Guéguen et al., 2011; Mundy et al., 2010), due in part to the remineralization of terrestrial organic carbon (OC_{terr}) supplied by rivers and coastal erosion. In the well-studied Siberian shelf seas, degradation of terrestrial organic carbon is a dominant control on acidification and CO_2 accumulation in surface waters (Semiletov et al., 2016). In the Arctic-outflow shelf sea Hudson Bay, in northern Canada (Fig. 1), strong links between $CaCO_3$ saturation (a measure of the tendency for $CaCO_3$ to dissolve; Azetsu-Scott et al., 2014), CO_2 air-sea flux (Else et al., 2008a, 2008b), and freshwater abundance have prompted speculation that CO_2 flux and OA are influenced by terrestrial carbon delivery and remineralization. However, no quantitative assessment of the potential effects of terrestrial carbon remineralization on CO_2 flux and OA has been undertaken to date. This budgeting exercise is complicated because the effects of terrestrial carbon delivery on OA and CO_2 flux may be partially offset by marine primary production and dissolution of

* Corresponding author.
E-mail address: david.capelle@umanitoba.ca (D.W. Capelle).

https://doi.org/10.1016/j.pocean.2020.102319
Received 5 June 2019; Received in revised form 20 December 2019; Accepted 31 March 2020
Available online 10 April 2020

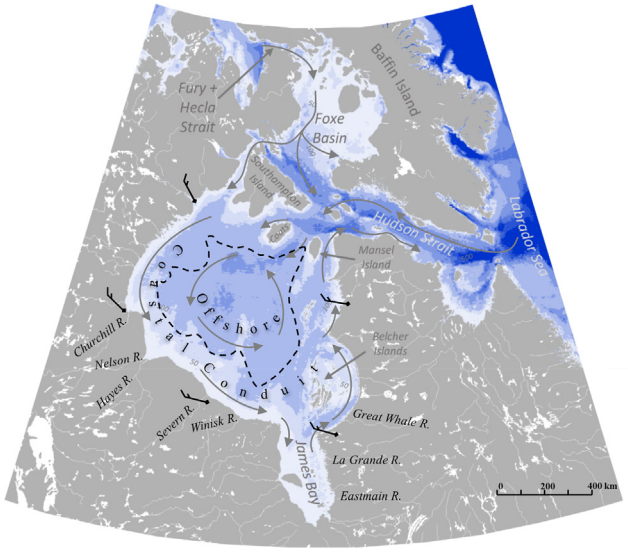

Fig. 1. Map of Hudson Bay showing bathymetry, circulation, major rivers, wind velocity, and boundary between coastal conduit and offshore domains as defined by current velocities in the NEMO ocean model. Grey arrows denote prevailing surface currents. The dashed line denotes the boundary between the runoff dominated coastal conduit and offshore region used in this study. Black flag-shaped symbols denote prevailing wind velocities.

terrestrial $CaCO_3$ in some regions, and exacerbated by the remineralization of marine organic carbon in others. Additional factors are also important, such as the delivery of freshwater from rivers and ice melt, which lowers the capacity of seawater to resist changes in pH. Understanding the key drivers of OA and CO_2 flux in high-latitude shelf seas is urgent in view of how rapidly these areas are responding to global warming, with many effects that potentially impact carbon cycling, including loss of permafrost, snow, and sea ice (Hochheim et al., 2014; Hochheim and Barber, 2010; Manizza et al., 2013), and changes in the magnitude and timing of river runoff (Dai et al., 2009; Déry et al., 2016). It is the sum total and balance of these changes that will determine the effects of ocean acidification and future air-sea CO_2 exchanges in these high-latitude northern seas.

Here, we take a step toward improving understanding of the key drivers of OA and CO_2 exchange in high-latitude Arctic shelf seas by examining the potential effects of important processes within the carbon system in the Hudson Bay system (HB). We first briefly review the main processes affecting air-sea CO_2 and OA in high-latitude seas. We then synthesize what is known about carbon cycling in this system, both organic and inorganic, to develop an integrated carbon budget that estimates annual supply and loss rates for various forms of carbon using a box model approach (Gordon et al., 1996). We use the box model to estimate the potential effects of terrestrial and marine organic carbon remineralization on OA and CO_2 flux, and the extent to which these effects may be enhanced or mitigated by marine primary production and $CaCO_3$ cycling. A sensitivity analysis reinforces the ability of the model (despite the uncertainties in some model assumptions) to identify key C-cycle-related drivers of OA and CO_2 flux in HB, and how these might be impacted by future changes (e.g., land-use and climate change). Finally, our results are used to evaluate potential drivers of OA and CO_2 flux in other high-latitude shelf seas.

Carbon cycling in high-latitude coastal oceans is complex because it involves both oceanic and terrestrial systems and because seasonal sea ice plays an important role (Fig. 2). River inflow and coastal erosion deliver organic carbon (OC) in dissolved (DOC) and particulate (POC) forms, as well as particulate and dissolved inorganic carbon (PIC and DIC) from the weathering of carbonate rocks and decomposition of terrestrial organic matter (Couture et al., 2018; Lantuit et al., 2012; Stein and Macdonald, 2004a; Vonk et al., 2015). Given our understanding of carbon cycling in other Arctic shelf seas (Bates, 2006; Kaltin and Anderson, 2005; McClelland et al., 2012; Shadwick et al., 2011; Shakhova et al., 2010), we know that seasonal OC_{mar} production is related to the dynamics of air-sea CO_2 flux and ocean acidification. However, the potential influence of OC_{terr} delivery by rivers and also PIC formation/dissolution has received limited attention in most high-latitude shelf seas.

A portion of the imported terrestrial OC (OC_{terr}) is remineralized biologically (Mann et al., 2012; Wickland et al., 2012), while some light-sensitive forms (chromophoric dissolved organic matter and fluorescent dissolved organic matter; CDOM and FDOM) may be photochemically oxidized, potentially providing a direct source of DIC (Bianchi, 2011; Granskog et al., 2009), or alternatively producing more labile (smaller) molecules (Dainard et al., 2015) and thus increasing bacterial remineralization rates (Amon, 2004). A fraction of the POC_{terr} discharged by rivers sinks rapidly to the bottom (seabed), where it may be remineralized to CO_2 if oxygen or other oxygen-bearing molecules are present, or to methane (CH_4) if sediments are anoxic (usually below the sediment surface in high-latitude coastal oceans). The remaining POC_{terr} that is not remineralized is buried, which sequesters carbon away from the atmosphere for thousands to millions of years.

The majority of CO_2 released by remineralization reacts with water to form carbonic acid (H_2CO_3), bicarbonate (HCO_3^-) and carbonate (CO_3^{2-}), as well as hydrogen ions (H^+) (Fig. 2). Thus, the CO_2 produced during remineralization of OC_{terr} increases the total dissolved inorganic carbon (DIC) content of the water column and lowers pH (i.e., promotes OA). As CO_2 and DIC accumulate, surface waters may become super-saturated in CO_2 and evade the excess CO_2 to the atmosphere, which mitigates OA. DIC and CO_2 may also be consumed by primary producers (phytoplankton, algae, and seagrasses) in sunlit waters during photosynthesis, potentially promoting CO_2 under-saturation and uptake of atmospheric CO_2.

Much of the organic matter produced by marine primary production (OM_{mar}) is recycled within the mixed layer (regenerated production) and thus only affects OA and CO_2 flux on seasonal scales. However, the portion that sinks to deeper waters (i.e., export production) effectively reduces the CO_2 concentration and effects on OA in surface waters. Export production is supported by nutrient delivery to the surface mixed layer from upwelling of deeper waters, rivers, and remineralization of terrestrial organic matter (Eppley and Peterson, 1979). Some of the OC_{mar} exported to deeper waters is remineralized, contributing to OA and CO_2 accumulation in deep waters, while the remainder is buried in sediments.

Particulate inorganic carbon (PIC; i.e., $CaCO_3$) is a solid mineral that may be formed through the combination of dissolved calcium (Ca^{2+}) and HCO_3^- (Fig. 2) by marine organisms (e.g., some phytoplankton, clams, mussels). In river waters, PIC can also derive from physical weathering of carbonate-containing rocks, and in the ocean, sea-ice formation can lead to the production of an abiotic form of $CaCO_3$, ikaite (Dieckmann et al., 2010). The tendency for calcium carbonate to dissolve in seawater is defined by Ω, which depends on the concentration of calcium and carbonate ions, as well as the temperature, salinity, and hydrostatic pressure and the mineral structure of solid $CaCO_3$ (for more details see AMAP, 2013). PIC is stable in most surface ocean waters (i.e., $\Omega > 1$), but the addition of CO_2 promotes $CaCO_3$-dissolution (i.e., $\Omega < 1$), which is a main concern resulting from ocean acidification, as it may stress shell-producing organisms. Of the two major forms of marine carbonate used by aquatic organisms, aragonite and calcite, the former is more soluble and therefore more sensitive to ocean acidification. Calcium-carbonate dissolution consumes CO_2, reducing the potential for CO_2 outgassing (Fig. 2) and increases the aragonite saturation state (Ω_{Ar}; AMAP, 2013), potentially offsetting the effects of organic matter remineralization.

Freshwater has a significant influence on the buffering capacity of high-latitude shelf waters (i.e., their ability to resist changes in pH resulting from CO_2 addition or removal). Most river waters have a low

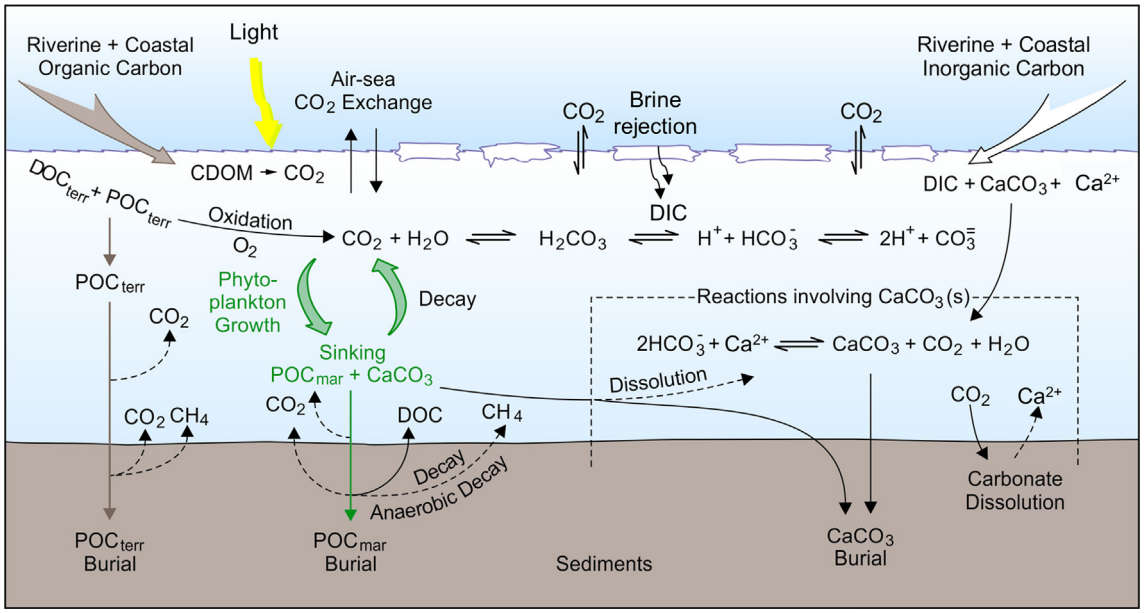

Fig. 2. Schematic showing major processes related to the carbon cycle in high-latitude shelf seas.

buffering capacity, as indicated by them having a lower total alkalinity (TA) than seawater. Thus, river-dominated coastal marine waters are more vulnerable to OA than their more saline offshore counterparts (AMAP, 2013). Like river water, sea-ice melt has relatively low TA, further contributing seasonally to the OA vulnerability of high-latitude seas (Carmack et al., 2016).

Sea ice also affects the carbon cycle in high-latitude seas in other ways. Drifting sea ice transports particulate organic and inorganic matter together with sediment. Sea-ice cover impedes direct air-sea CO_2 exchange. Brine rejection during ice formation may export salts and other components including carbon, down and away from the surface and in some cases to deep waters (Fig. 2; König et al., 2018; Moreau et al., 2016; Rysgaard et al., 2011). In the absence of deep mixing or bottom-water formation, the DIC in deep waters remains isolated from the surface layer and atmosphere for decades (as expected for Hudson Bay) to hundreds of years (for the Arctic Ocean; Östlund et al., 1987). The specific carbon cycling processes within sea ice are complicated and this remains an area of on-going research (e.g. Brown et al., 2015; Else et al., 2012; Geilfus et al., 2014; Rysgaard et al., 2011; Vancoppenolle et al., 2013).

Fig. 2 emphasizes that the total inventories and exchanges of carbon between the various compartments of a high-latitude coastal ocean system are dynamic and driven by a combination of physical, chemical, and biological processes, all of which may vary regionally in space, and seasonally, annually, or on longer time scales. The Arctic already shows many signs of global change, including warming (AMAP, 2017), reduced sea-ice cover (Hochheim et al., 2014; Kwok et al., 2009; Stroeve and Serreze, 2008), and changing freshwater flux from rivers (Dai et al., 2009; Déry et al., 2016). It remains to be determined how these changes will enhance or mitigate rates of air-sea CO_2 flux and acidification.

2. Methods

2.1. Study area

Hudson Bay (HB) is a large, shallow, semi-enclosed sea, with a complete cryogenic cycle (ice covered in winter, open water in late summer). Like the Arctic Ocean, Hudson Bay receives more river water input per unit area than other ocean regions. Pacific-derived, relatively fresh Arctic Ocean outflow enters Hudson Bay from the north via both Hecla and Fury Strait and northern Hudson Strait (Fig. 1), and circulates cyclonically around the Bay in the so-called 'coastal conduit' that is mostly confined to within 100 km of the shoreline (Granskog et al., 2009). Here, surface marine water is modified by dilution with river water and biogeochemical processes before eventually exiting Hudson Bay via southern Hudson Strait and flowing into the Labrador Sea (Fig. 1). Most of the river water and associated terrestrial carbon enters along the Bay's southern coast from the Churchill and Nelson Rivers in the southwest, to the La Grande and Great Whale Rivers in the southeast. Significant advances have been made in understanding specific aspects of the HB carbon cycle during the last 15 years (ArcticNet research program), including marine primary production, organic carbon delivery and burial, CO_2 flux, and aragonite-saturation, but these findings have not, to date, been integrated into an overall picture of carbon cycling in Hudson Bay and its implications for OA and CO_2 flux.

2.2. Overall model structure

We subdivide HB into a *coastal* box and an *offshore* box, each of which is further divided into a *surface* box and *deep* box. The boundary between surface and deep boxes is assumed to average about 50 m, consistent with the approximate depth of the HB mixed layer (Granskog et al., 2009; Saucier et al., 2004). The boundary between the coastal and offshore domains (dashed line in Fig. 1) is defined based on surface currents projected from the HYPE model (N. Ridenour, *pers. comm.*), giving a coastal surface area of 557,000 km^2 and an offshore surface area of 250,000 km^2 (see Table SI-1). This boundary is also consistent with the distribution of river water, which dominates within 100–150 km of the HB coast, based on both water-mass tracers (Granskog et al., 2011, 2009, 2007) and models (St-Laurent et al., 2011). We use previously published and recent measurements to estimate the carbon fluxes in and out of each box, and transformations within each box (see Table SI-1). Note that much of the observational data available from Hudson Bay is biased towards the open water season (summer and fall), when the absence of ice cover makes field programs practical. Where suitable data were not available, we used relevant literature from elsewhere and/or assigned fluxes to balance inputs and outputs within reasonable error estimates. We also conduct a sensitivity analysis to determine how uncertainties within the model affect our results.

2.3. Effects of C-cycle processes on ocean acidification and air-sea CO_2 flux

We assess the effects of specific C-cycling processes on OA and air-sea CO_2 flux in HB by calculating their annual effects on the average Ω_{Ar} and pCO_2 in each compartment using the CO2SYS program (Pierrot and Wallace, 2006). We are interested in the changes in these properties brought about by C transformations in HB and thereby imparted to the outflowing waters (towards the Labrador Sea), relative to Arctic waters that do not pass through the HB system on their way to the Labrador Sea. CO2SYS calculates Ω_{Ar} and pCO_2 (among several other parameters, including pH, saturation states for other minerals, etc.) using a set of water chemistry variables (salinity, temperature, pressure, total phosphate, total silicate, total alkalinity, and total dissolved inorganic carbon). We estimate the average set of water chemistry variables in each of our four compartments based on existing literature to derive average Ω_{Ar} and pCO_2 values using CO2SYS (see Table SI-2). We then infer the effects of carbon transformations (i.e., remineralization of POC_{terr}, DOC_{terr}, and POC_{mar}, marine primary production, and PIC_{terr} dissolution) on this set of water chemistry variables, based on our carbon budget and stoichiometric relationships between carbon and other variables. This modelling experiment allows us to derive the annual contributions of specific carbon cycle processes to the mean pCO_2 and Ω_{Ar} in each compartment of our box model and thus compare relative contributions and identify key driving and offsetting processes.

We convert DIC from teragrams (Tg $= 1 \times 10^{12}$ g; the units used throughout the budget) to molar concentrations by dividing the Tg DIC changes in each box by the total volume of each compartment in our budget. Compartment volumes were derived from the surface areas of the coastal (579,000 km^2) and offshore (251,000 km^2) regions, and average thicknesses of each compartment (50 m for the two surface boxes, 50 m for the deep coastal box, and 150 m for the deep offshore box based on the approximate mean depth of each compartment from bathymetric maps).

Next, we derive changes in other relevant CO2SYS inputs based on DIC. The change in DIC due to remineralization/primary production is related to changes in TA by:

$$\Delta TA_{PP/reminOMmar} = \frac{-16}{106} \times \Delta DIC_{PP/reminOMmar} \quad (2.3.1)$$

where delta $\Delta TA_{PP/reminOMmar}$ and $\Delta DIC_{PP/reminOMmar}$ are the net change in total alkalinity and dissolved inorganic carbon, respectively, due to primary production and remineralization of marine organic matter. The -16:106 conversion factor is due to the uptake/release of nitrate (NO_3^-) during primary production/remineralization, which affects TA (Sarmiento and Gruber, 2006). Thus, for every mole of DIC produced during remineralization, TA is reduced by a factor of 16:106. However, based on observations from 15 rivers sampled during August 2011 (Table 1), the carbon to nitrogen (C:N) molar ratio of terrestrial organic matter (OM_{terr}) delivered by Hudson Bay rivers is higher than 106:16 (28.6:1 for dissolved OM_{terr} and 12.2:1 for particulate OM_{terr}). Thus, for every mole of DIC produced by DOM_{terr} remineralization, TA is reduced by a factor of 1:28.6, while this ratio would by 1:12.2 for POM_{terr} remineralization.

$$\Delta TA_{PP/reminOMterr} = \frac{-1}{28.6} \times \Delta DIC_{PP/reminDOMterr} \quad (2.3.2)$$

Similarly, the change in TA due to PIC precipitation and dissolution is related to DIC by:

$$\Delta TA_{PICpptn/dissol} = 2 \times \Delta DIC_{PICpptn/dissol} \quad (2.3.3)$$

where $\Delta TA_{PICform/dissol}$ and $\Delta DIC_{PICform/dissol}$ are the net changes in total alkalinity and DIC from the formation and dissolution of PIC (Sarmiento and Gruber, 2006). Because TA depends on the total ionic charge of its constituent ions, whereas DIC does not, the production of CO_3^{2-} during PIC dissolution increases TA by a factor of two, relative to the increase in DIC (Zeebe and Wolf-Gladrow, 2001).

A similar approach was used to infer changes in total phosphorus. We adjusted for different sources of organic matter, assuming the N:P ratios of OM_{terr} and OM_{mar} were always 16:1 (Loladze and Elser, 2011; Redfield, 1934). Thus, for every mole of DIC produced by OM_{mar} remineralization, PO_4^{3-} increases by 1/106, and for every mole of DIC from particulate OM_{terr}, PO_4^{3-} increases by 1/458 (equivalent to a C:N of 28.6:1, and N:P = 16:1).

Silicate concentrations may be affected by remineralization and primary production if silicate forming organisms are present. However, the lack of published silicate concentration data precludes an accurate constraint of this factor in HB, so we simply assume Si remains constant in each box. Salinity, temperature, and pressure were also assumed to be unaffected by C-cycling.

We then re-calculate the pCO_2 and aragonite-saturation values for each compartment after modifying the average DIC, TA, and phosphorus values by the amounts inferred from the annual carbon budget and the stoichiometric relationships discussed above. The difference between this Ω_{Ar} and pCO_2 value and the original values is equivalent to the annual effects of a given C-transformation, while their sum provides an estimate of the net effect of C-cycling on Ω_{Ar} and pCO_2 in each compartment.

3. Synthesis of Hudson Bay carbon literature and box model formulation

To formulate our budget, we have drawn on several studies examining specific aspects of the HB C-system including both the inorganic C system (Azetsu-Scott et al., 2014; Burt et al., 2016; Else et al., 2008a, 2008b) and the organic C system (Ferland et al., 2011; Godin et al., 2017; Granskog et al., 2007; Guéguen et al., 2011; Kuzyk et al., 2010, 2009, 2008; Lapoussière et al., 2013, 2009; Mundy et al., 2010). Below, we show first the terrestrial organic carbon budget (inputs, losses, and transformations), followed by the marine organic carbon budget, and finally the inorganic carbon budget.

3.1. Terrestrial POC budget

Rivers are a large source of POC_{terr} to HB, as they are to other river-dominated shelf seas. For our POC_{terr} budget, we adopt the estimates made by Kuzyk et al. (2009), who showed that rivers, coastal erosion and atmospheric dust deposition supply an estimated 0.46 Tg/yr, 0.07 Tg/yr and 0.125 Tg/yr POC_{terr} to the HB system, respectively. We assume river waters and coastal erosion enter directly into the coastal region. In contrast, dust is deposited evenly across the surface area of the Bay, implying 0.09 and 0.04 Tg/y to the coastal and offshore waters, respectively (Fig. 3). The amount of POC_{terr} delivered to Hudson Bay on an areal basis (0.6 g m^{-2}) is comparable to the amount estimated for the Arctic Ocean (1.1 g m^{-2}; Stein and Macdonald, 2004a, 2004b), with the result that bottom sediments from both areas are noticeably “terrestrial” in their organic matter (Kuzyk et al., 2009; Schubert and Calvert, 2001).

The burial rates of POC_{terr} are estimated from sediment cores (Kuzyk et al., 2009, 2010), and display marked regional variability depending on distance from shore. Terrestrial organic matter (OM_{terr}) supplied by rivers to HB is generally nitrogen-poor relative to OM_{mar}, with a C:N ratio of 28.6:1 for DOC and 12.2:1 for POC (Table 1). The spatial patterns in C:N ratios of HB bed sediments suggest that OM_{terr} is primarily deposited in coastal waters near major rivers (Churchill/Nelson, James Bay rivers) in the southern part of the Bay (Kuzyk et al., 2010). Lignin yields from riverine particulate matter and sediment cores confirm the general pattern of a coastal current transporting fine sediments and OC_{terr} cyclonically around the margin of the Bay, with the majority of OC_{terr} deposited within the coastal zone (Godin et al., 2017; Kuzyk et al., 2008). Kuzyk et al. (2009) estimated that OC_{terr} makes up roughly 40% of the total OC in coastal sediments, but only ~7% in offshore sediments, implying total OC_{terr} delivery rates of 0.44

Table 1
Carbon:Nitrogen ratios of POM and DOM measured at the mouth of 15 Hudson Bay rivers during August 2011.

River	Latitude	Longitude	Sampling Date (Day of Year)	Drainage Basin Area (km^2)	Annual Q (km^3/yr)	Peak Flow (Day of Year)	C:N of POC	C:N of DOC
East								
Povungnituk	60.05	77.22	191	28,000	11.9	184	13.5	23.4
Kogaluk	59.61	77.48	191	11,300	5.0	171	16.3	26.7
Polemud	59.43	77.30	191	N/A	1.5	170	14.0	29.0
Innuksuak	58.46	78.08	192	11,200	3.3	174	12.8	36.8
Nastapoca	56.92	76.43	193	12,500	8.0	173	13.2	22.6
Little Whale	55.97	76.67	193	11,700	3.7	164	13.7	24.9
Great Whale	55.27	77.57	194	43,200	19.8	153	10.8	37.1
Northwest								
Josephine	63.13	90.98	199	N/A	2.5	180	9.2	20.1
Wilson	62.33	93.13	199	N/A	2.6	180	11.0	22.3
Ferguson	62.08	93.35	199	12,400	2.6	181	12.8	31.2
Tha'anne	60.55	94.92	200	29,400	6.3	175	8.7	22.8
Thlewiaza	60.52	95.02	200	27,000	6.9	183	12.1	29.0
Southwest								
Churchill	58.78	94.20	201	288,880	20.6	161	10.2	27.9
Severn	55.87	87.82	209	94,300	21.3	149	11.9	35.0
Winisk	55.15	85.30	209	54,710	14.7	148	12.5	40.4
Average							**12.2**	**28.6**

and 0.01 Tg C y^{-1} to the coastal and offshore sediments, respectively (Fig. 3). The difference between OC_{terr} supply and burial in sediments implies water-column remineralization rates of 0.18 (coast) and 0.028 Tg C y^{-1} (offshore). Lacking detailed measurements about POC sinking and remineralization rates, we have simply partitioned the remineralization of POC_{terr} evenly between the mixed layers and deeper waters of the coastal and offshore regions (Fig. 3).

Remineralization can also occur within sediments, after deposition. Based on the difference between OC in surface vs. deeper sediments, Kuzyk et al. (2009) showed that ~39% of the OC_{terr} reaching the sediments is remineralized, which would release 0.18 and 0.004 Tg C y^{-1} as DIC to the coastal and offshore bottom waters, respectively (Fig. 3; Kuzyk et al., 2009). Overall, our budget suggests that only 42% (0.28 Tg) of the total annual POC_{terr} delivered to HB (0.66 Tg) is permanently buried with the remaining 58% remineralized in the water column and sediments.

3.2. Terrestrial DOC budget

Rivers supply HB with even greater amounts of DOC_{terr} than POC_{terr},. Thus, we expect that HB surface waters also contain relatively high concentrations of DOC. The links between river runoff and DOC distribution in HB have been defined largely through trends in the chromophoric portion (CDOM) (Mundy et al., 2010; Granskog et al., 2007; Guéguen et al., 2011). The concentration of CDOM in Hudson Bay mixed-layer waters is equal to or greater than that in the Beaufort Sea or Mackenzie River Delta and considerably greater than in the Greenland Sea or central Arctic Ocean (Pegau, 2002; Stedmon and Markager, 2001). Delivery of DOC_{terr} and $CDOM_{terr}$ by rivers to HB varies considerably from low levels in the northern rivers to higher levels in the southern and western rivers draining the Hudson Bay Lowlands (peatlands) (Godin et al., 2017). Seasonal fluctuations in DOC concentrations are significant in some rivers but not others (Kirk and Louis, 2009; Rosa et al., 2012). However, only a handful of rivers have been monitored throughout an annual cycle, preventing

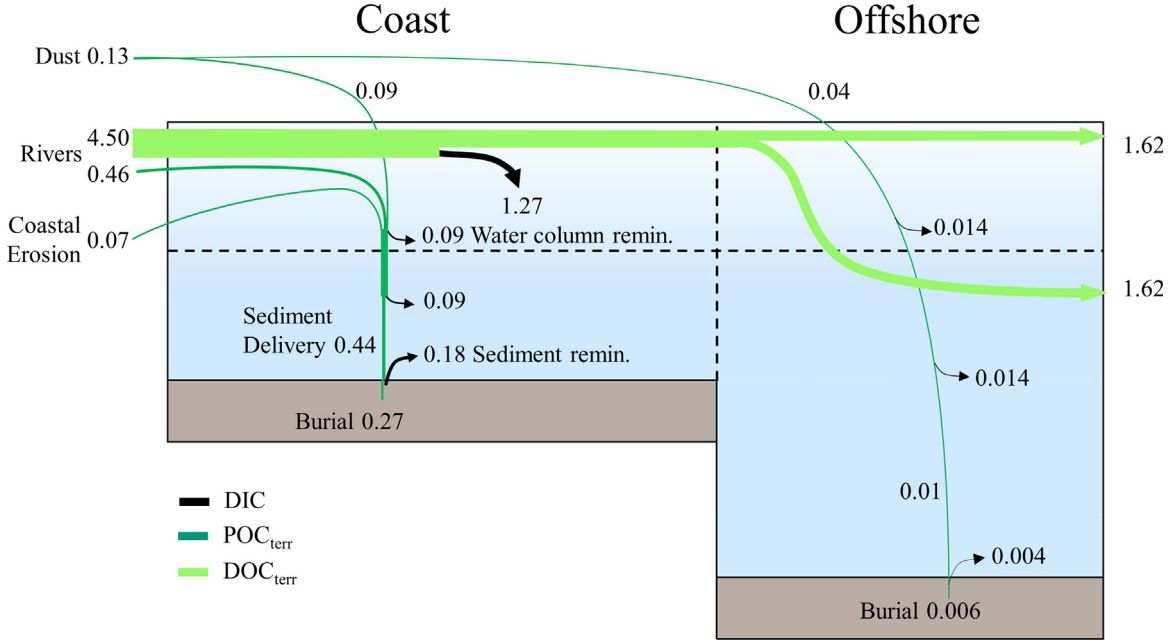

Fig. 3. Terrestrial carbon budget for Hudson Bay. Light green indicates DOC_{terr}, dark green is POC_{terr}, and black represents the formation of DIC through remineralization. The units are Tg C y^{-1}.

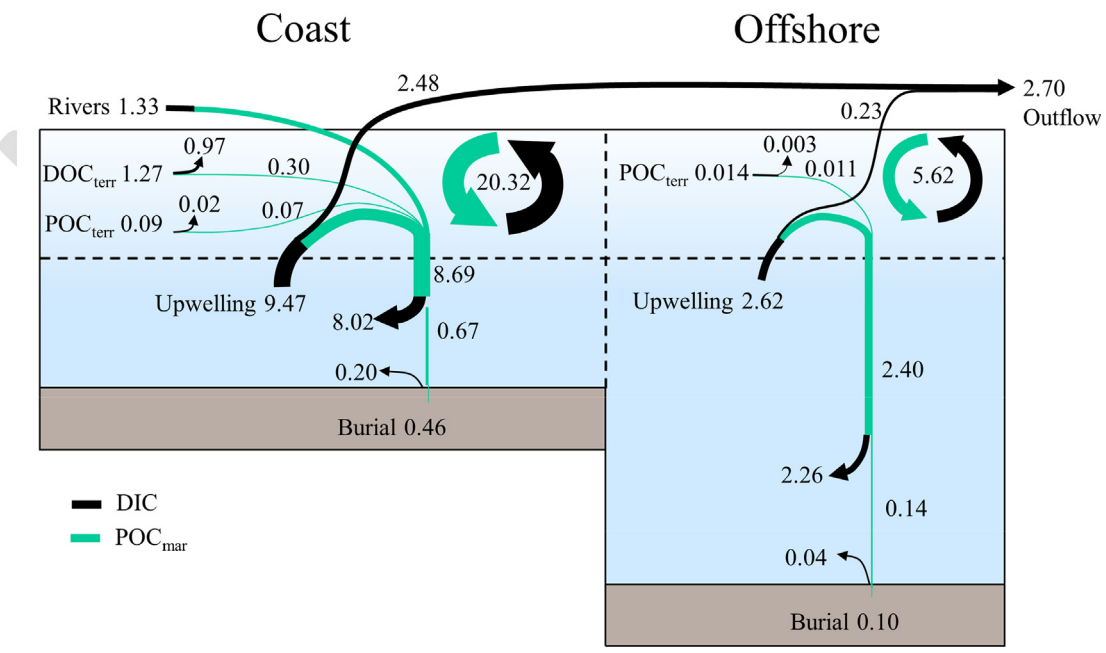

Fig. 4. Marine carbon budget for HB. Black arrows represent DIC from remineralization of organic matter, and green arrows represent the marine organic carbon. Units are Tg C y^{-1}.

generalizations. Furthermore, the DOC data for the marine waters are too scarce to resolve potential spatial differences in DOC loading at the present time beyond an inshore/offshore contrast. The pronounced inshore-offshore gradients in absorbance at 355 nm (*a*355) confirm that the coastal waters are dominated by $CDOM_{terr}$-rich river waters (Granskog et al., 2007). The only published estimates suggest that Hudson Bay receives between 3.6 and 5.5 Tg C y^{-1} as DOC_{terr} (Kuzyk et al., 2009; Mundy et al., 2010). Thus, for our box model, we adopt a mean value of 4.5 Tg C y^{-1} for DOC_{terr} delivery by rivers to the coastal surface HB compartment (Fig. 3). This input is nearly an order of magnitude larger than the estimated input of POC_{terr} (Fig. 3). There are presently no published estimates of DOC delivery from coastal erosion to Hudson Bay, and we assumed this to be of minor importance because isostatic rebound in Hudson Bay is greater than the rate of sea-level rise (Hillaire-Marcel and Fairbridge, 1978).

Dissolved organic carbon can be remineralized by photochemical (Timko et al., 2015) and bacterial processes (Catalá et al., 2015; Guéguen et al., 2014; Walker et al., 2016). The biodegradable fraction of DOC_{terr} varies seasonally, with more labile DOC_{terr} behaviour during winter (Wickland et al., 2012) or the spring freshet (Holmes et al., 2008) than during other seasons. The degradability of DOC_{terr} also depends on its sensitivity to light and chemical structure, which varies with watershed characteristics (cf., Godin et al., 2017). In general, the fraction of DOC_{terr} that is degraded in marine waters does not exceed 25–30% (Bauer and Bianchi, 2012). Based on generally conservative relationships between salinity and *a*355 in Hudson Bay, early studies on $CDOM_{terr}$ in HB suggested low rates of degradation (Granskog et al., 2007). However, the optically active fraction of DOC (both absorbing and fluorescing) is particularly high in Hudson Bay (up to 89%), suggesting DOC may be particularly photolabile (Guéguen et al., 2011). Rapid DOM_{terr} losses of *a*355 over two-day light exposure experiments (61–68%, 49–56% and 52% for river, estuarine and offshore samples, respectively; Guéguen et al., 2016) suggest that much of the DOC from rivers is photochemically degraded in nearshore waters, which may increase the lability of DOM_{terr} and promote microbial degradation (Bianchi, 2011).

Given the potential variability in DOC_{terr} degradability and paucity of published data, we adopt the formulation devised by Wickland et al. (2012) for estimating the fraction of DOC_{terr} that can be remineralized to DIC in HB. This estimate is based on the ratio of DOC and dissolved inorganic nitrogen (DIN) of rivers:

$$ln\%BDOC = (-0.589 \times \ln(DOC{:}\ DIN)) + 5.17 \quad (3.2.1)$$

where %BDOC is the percentage of the total DOC that is biodegradable and DIN is the sum of nitrate (NO_3^-) and ammonium (NH_4). HB rivers have mean NO_3^- concentrations of 3.7 ± 2.1 μmol L^{-1} (Kuzyk et al., 2010), but NH_4 data are more limited. Measurements of NO_3^- and NH_4 from the lower Nelson River (n = 16) spanning multiple seasons showed a mean NH_4:NO_3^- ratio of 4:1 (Baker, 1989). We used this ratio to derive the mean river DIN (18.5 μmol L^{-1}) from the mean river NO_3^-. We then applied the Wickland et al. (2012) equation to Hudson Bay, assuming a mean river DOC concentration of 414 μmol L^{-1}, which we derived by dividing the total DOC supply (4.5 Tg C y^{-1}) by the total annual river discharge (905 km^3 y^{-1}; SI-Table 1). The result suggests that ~28% (1.27 Tg) of the DOC_{terr} delivered by HB rivers is remineralized to DIC in Hudson Bay (Fig. 3). This degree of degradability is higher than observed for the Kolyma River (0.1–20%; Mann et al., 2012) or for a temperate estuary (10%; Raymond and Bauer, 2000) but lies at the upper end of ranges observed for three large Alaskan rivers (0–33%; Holmes et al., 2008). Given that DOC_{terr} is associated with river water which is mostly confined to the coastal surface waters in HB (Granskog et al., 2011), and that most DOC_{terr} degradation typically occurs within days to weeks (Herlemann et al., 2014; Kawahigashi et al., 2004) (i.e., before river water would mix with subsurface (> 50 m deep) and offshore waters) we apply this DOC_{terr} remineralization rate (28%) to the surface coastal compartment of our box model (Fig. 3).

3.3. Marine POC budget

Hudson Bay has long been considered an oligotrophic system with low primary production (Anderson and Roff, 1980; Dunbar, 1993; Ferland et al., 2011; Lapoussière et al., 2013; Roff and Legendre, 1986), although the main spring phytoplankton bloom has yet to be assessed. Estimates of annual primary production in Hudson Bay vary from 10 to 100 g C m^{-2} yr^{-1} (Anderson and Roff, 1980; Ferland et al., 2011; Lapoussière et al., 2013; Roff and Legendre, 1986; Sibert et al., 2011), but the bulk of the evidence supports the lower end of the range.

For the marine OC budget (Fig. 4), we require estimates of new primary production or export production (i.e., the portion of marine carbon exported from the surface mixed layer). Within Hudson Bay, field observations consistently show a general decline in productivity and biomass from the coast to offshore waters, and from northeast to southwest (Ferland et al., 2011; Lapoussière et al., 2013). Spatial differences in sediment dinoflagellate cyst assemblages (Heikkilä et al., 2016, 2014) display a higher abundance of the spring bloom-associated *Pentapharsodinium dalei* in eastern HB where they may be supported by abundant nutrients associated with strong river inflows (Kuzyk et al., 2010), whereas the central and western regions are characterized by slower-growing plankton, both autotrophs and heterotrophic dinoflagellates, perhaps due to longer periods of sea-ice cover and oligotrophy. There is potential for significant primary production contributions from both ice algae (Cota et al., 1991) and benthic primary producers (Lalumière et al., 1994; Welch et al., 1991), but field observations have so far failed to capture these. In contrast to field observations, a 3D physical-biogeochemical model showed no indication of elevated primary production inshore, which was attributed to light limitation from high particulate and dissolved organic matter loadings from rivers (Sibert et al., 2011).

Given the uncertainties in primary production estimates from field observations and models, we chose to estimate export production by using a geochemical budget for dissolved inorganic nitrogen (DIN). Export production is the most important component of primary production in terms of affecting OA and the air-sea exchange of CO_2, because export production removes CO_2 from the surface for more than a season and contributes CO_2 to deep water through POC_{mar} remineralization. The premise here is that export production must be supported by the import of bioavailable nitrogen to the mixed layer, either by remineralization of terrestrial organic matter (OM_{terr}), direct DIN supply from rivers, or upwelling of sub-surface seawater.

We estimate the export production supported by OM_{terr} remineralization based on the remineralization of POC_{terr} and DOC_{terr} in the surface boxes (Fig. 3) and the corresponding release of nutrients based on the C:N ratios of DOM_{terr} and POM_{terr} (Table 1). Note we assume the C:N ratios of dust and coastal erosion are the same as POM_{terr} in rivers. Assuming that marine primary producers consume C:N at Redfield ratios (106:16), the nutrients released by DOM_{terr} remineralization could support 0.30 Tg C y^{-1} export production in the coastal surface box, which offsets ~25% of the DIC released by DOM_{terr} remineralization. In contrast, the nitrogen released from POM_{terr} remineralization would support 0.07 Tg C y^{-1} export production in the coastal surface box, or nearly 80% of the DIC from POC_{terr} remineralization (Fig. 4).

To estimate the export production supported by river DIN, we multiply the mean river DIN concentration (18.5 μmol L^{-1}) by the mean annual river discharge (905 km^3 y^{-1}; McCullough et al., 2019, Table SI-1), which gives a total annual DIN supply of 0.23 Tg N/yr. This supports 1.33 Tg C y^{-1} export production (Fig. 4). We assume that the river DIN is derived from OM_{terr} remineralization upstream, and thus associated with DIC delivery by river water. Assuming a 28.6:1 C:N ratio as an upper limit for OM_{terr} (Table 1), river DIN may be associated with up to 5.83 Tg C y^{-1} as DIC. However, much of this DIC is likely lost to the atmosphere as CO_2 before reaching HB, as many Arctic rivers are strong CO_2 sources in the upper watershed but become weak sources or sometimes even CO_2 sinks in the lower reaches near the river mouth (Denfeld et al., 2013; Striegl et al., 2012). Many of the large river systems of HB (Nelson, La Grande) have lakes or reservoirs that support primary production themselves. Accordingly, we adopt a lower limit for river DIC:DIN ratios by assuming that the remineralized DIC imported by rivers is present at the same 106 C:16 N ratio as marine organic matter, for a total supply of 1.33 Tg C y^{-1}. As a result, the export production supported by river DIN would consume all associated river DIC (Fig. 4).

To estimate the export production supported by upwelled nitrogen, we constructed a salt budget based on mean annual river runoff (905 km^3 y^{-1}), the salinity of outflowing water to Hudson Strait (30.78; average salinity of upper 50 m in northeastern HB near Hudson Strait), and the salinity of water upwelled to the surface of Hudson Bay (32.80; average salinity of water below 50 m depth). The salinity of outflowing water suggests that it is composed of 94% upwelled water and 6% freshwater. Assuming the river-water inflows are balanced by an equal volume of river water flowing out of HB each year, we infer that ~15,100 km^3 y^{-1} of upwelling is required to balance the salt budget (Table SI-1). We multiply this volume flux by the average DIN concentrations in upwelled water based on previously collected measurements (10.1 μmol L^{-1}; n = 5), and the DIN in outflowing surface waters near the mouth of Hudson Bay (2.1 μmol L^{-1}) to infer the total supply of DIN to the surface and loss in outflowing waters. The total DIN upwelled in HB could support 12.1 Tg C export production per year, but 2.7 Tg of this DIN leaves with outflow to Hudson Strait, producing a net 11.1 Tg C y^{-1} export production term. Given the larger surface area of the coastal region (~2x larger) and higher rates of primary production (~2x higher) relative to offshore waters (Ferland et al., 2011), the export production in the coastal box is assumed to be roughly 4x higher than the offshore. Accordingly, we apportion 8.69 Tg C y^{-1} of the net export production from upwelling to the coastal domain, along with 2.5 of the 2.7 Tg C lost due to outflow, with the remaining export production (2.4 Tg C y^{-1}) and outflow losses (0.23 Tg C y^{-1}) to the interior (Fig. 4).

Field observations show that export production makes up 30% of the total annual primary production in HB (Ferland et al., 2011; Lapoussière et al., 2013), which we use to estimate total annual primary production (37.1 Tg C y^{-1}) and regenerated production (26.0 Tg C y^{-1}) from our export production term (Fig. 4). The average annual primary production rate (44.7 g C m^{-2} y^{-1}) falls within the range of published estimates for Hudson Bay (10–100 g C m^{-2} y^{-1}; Anderson and Roff, 1980; Ferland et al., 2011; Lapoussière et al., 2013; Roff and Legendre, 1986; Sibert et al., 2011).

The remineralization of sinking marine OC in the water column was derived by subtracting the amount of marine POC reaching sediments (0.67 and 0.14 Tg y^{-1} in the coastal and offshore domains, respectively; Kuzyk et al., 2009) from the total export production terms. The difference implies that 8.02 and 2.26 Tg C y^{-1} of export production are remineralized in the coastal and offshore water columns, respectively (Fig. 4). We assume that the recycled primary production consists of a mixture of POC and DOC, but that no marine DOC is exported below the mixed layer, since marine DOC is highly labile (Holding et al., 2017; Retelletti Brogi et al., 2018) and thus rapidly remineralized in the ocean (within hours to days; Hansell, 2013). Roughly 30% of the OC_{mar} reaching sediments is remineralized (Kuzyk et al., 2009), releasing an additional 0.2 and 0.04 Tg DIC to coastal and offshore bottom waters, respectively (Fig. 4). Overall, this suggests that 10.7 Tg (i.e. > 95%) of the sinking marine organic matter is remineralized rather than buried, as compared to ~30% remineralization for DOC_{terr} and ~60% remineralization for POC_{terr}.

3.4. Particulate inorganic carbon budget

Little is known about production, distribution or dissolution of particulate inorganic carbon (PIC) in Hudson Bay, despite its potential effect on pH and pCO_2 (cf., Azetsu-Scott et al., 2014). Using available datasets from the Nelson, Hayes, Eastmain and La Grande Rivers (Table 2), we estimate an annual river PIC delivery of 1.2 Tg C y^{-1} (Fig. 5). The annual contributions of each river are based on their PIC concentrations and annual discharge, and we assume the PIC concentration from all unstudied rivers are equal to the average PIC concentration of the measured rivers. Coastal erosion is estimated to supply an additional 0.2 Tg C y^{-1} as PIC to the coastal box by assuming 2.5% inorganic carbon content in the sediment supplied by this source. Given the absence of information about PIC delivery by dust to HB, and relatively insignificant contribution of dust to the POC budget, we assume

Table 2
River PIC flux data. Annual fluxes were estimated by multiplying concentrations by annual discharge values. We used the average river PIC value for all other rivers not measured directly, multiplied by the remaining annual discharge from rivers not shown in the table. The Nelson and Hayes Rivers were measured by Stainton, M. The Eastmain and La Grande Rivers were averaged over the period 1982–1984.

River	Discharge ($km^3\ y^{-1}$)	PIC ($mg\ L^{-1}$)	PIC flux ($Tg\ y^{-1}$)
Nelson (n = 7)	94.1	1.0	0.09
Hayes	18.6	0.8	0.01
Eastmain (n = 31)[1]	13	1.7	0.02
La Grande (n = 35)[1]	80.5	1.7	0.14
All Other Rivers	698.8	1.3	0.90
TOTAL RIVER PIC			1.2

[1] From Messier et al. (1986).

no annual PIC delivery by dust.

Sediment cores suggest the PIC burial rate is 0.1 Tg C y^{-1} in coastal sediments and 0.3 Tg y^{-1} in the offshore region (Kuzyk et al., 2009; Fig. 5). This implies either a significant amount of PIC formation in the offshore domain by pelagic organisms, or lateral transport of PIC from the coast to the offshore domain. Coccolithophores are capable of producing $CaCO_3$, but these organisms have not been found in HB in any appreciable quantities. Calcareous foraminifera are found in sediments but show a decline in abundance over time, possibly due to reduced preservation of more recent deposits (Griffiths, 2010). $CaCO_3$-shell forming animals are present in the sediments of HB, but mostly confined to nearshore sediments. On the other hand, suspension and lateral transport of sediment from the coast to the offshore region may be significant in HB (Kuzyk et al., 2009). We therefore assume that all the PIC in HB sediments is derived from rivers and coastal erosion. Assuming no PIC dissolution occurs in the deep offshore waters, only 0.3 Tg of the 1.4 Tg PIC delivered to the coast would need to be transported offshore. However, a lack of PIC dissolution in the offshore region seems unlikely, given the fact that offshore bottom waters are relatively corrosive to $CaCO_3$ compared to coastal waters (Azetsu-Scott et al., 2014; Burt et al., 2016). We therefore adjusted the fraction of PIC exported from the coastal region until the PIC dissolution as a percentage of the PIC delivered to each compartment was roughly equal for both the coastal and offshore bottom waters (i.e. ~71% dissolution). This requires 1.05 Tg of PIC to be resuspended and deposited in offshore waters (Fig. 5), and implies PIC dissolution of 0.25 and 0.75 Tg C y^{-1} (roughly 70% of total PIC delivery) in the coastal and offshore deep waters, respectively (Fig. 5).

3.5. Dissolved inorganic carbon budget

Most of the DIC sources and sinks in each compartment of our box-model were derived from the remineralization of OC_{terr} and OC_{mar} and from PIC formation/dissolution (Sections 3.1–3.4). Briefly, we estimate that the production of DIC associated with OC_{terr} remineralization (both POC and DOC) within rivers adds 1.33 Tg C y^{-1} to the mixed layer of the coastal domain. The remineralization of OC_{terr} within HB releases 1.36 and 0.27 Tg DIC y^{-1} to the coastal surface- and bottom-waters, respectively, and 0.014 Tg and 0.018 Tg DIC y^{-1} to the offshore surface- and bottom-waters, respectively (Fig. 3). The DIN associated with OM_{terr} remineralization supports export production in the mixed layer boxes, which removes some but not all of this DIC, due to the lower C:N ratio of OM_{mar} relative to OM_{terr} (Fig. 4). Although upwelling promotes export production, it has ultimately no net effect on the DIC budget, since the C:N ratios of upwelled water are assumed to be the same as in OC_{mar}, although some of the upwelled DIC could promote local CO_2 outgassing to the atmosphere. In the deep-water boxes, remineralization of sinking OC (terrestrial and marine) produces DIC in both the water column and sediments. The dissolution of sinking PIC from terrestrial sources releases DIC in deep boxes (Fig. 5).

Adding up the DIC accumulation in surface boxes from Fig. 4 suggests that coastal waters could release as much as 1.0 Tg C as CO_2 per year, while the limited DIC accumulation in offshore surface waters would not support any significant CO_2 evasion on annual time-scales. This agrees relatively well with the estimated annual CO_2 emissions of ~1.4 Tg C as CO_2 per year, primarily from coastal waters (Else et al., 2008b). However, we intentionally excluded air-sea CO_2 flux from the budget because it would remove some of the CO_2 added by OM remineralization, and thus offset the potential effects on Ω_{Ar}. Our budget thus provides an indication of the potential tendency for surface waters to be sources or sinks for atmospheric CO_2.

3.6. Contributions of carbon transformations to pCO_2 and Ω_{Ar}

The effects of individual carbon transformations on mean Ω_{Ar} (Fig. 6a) and pCO_2 (Fig. 6b) in each box model compartment are discussed below. We investigate the effects of POC_{terr} and DOC_{terr}

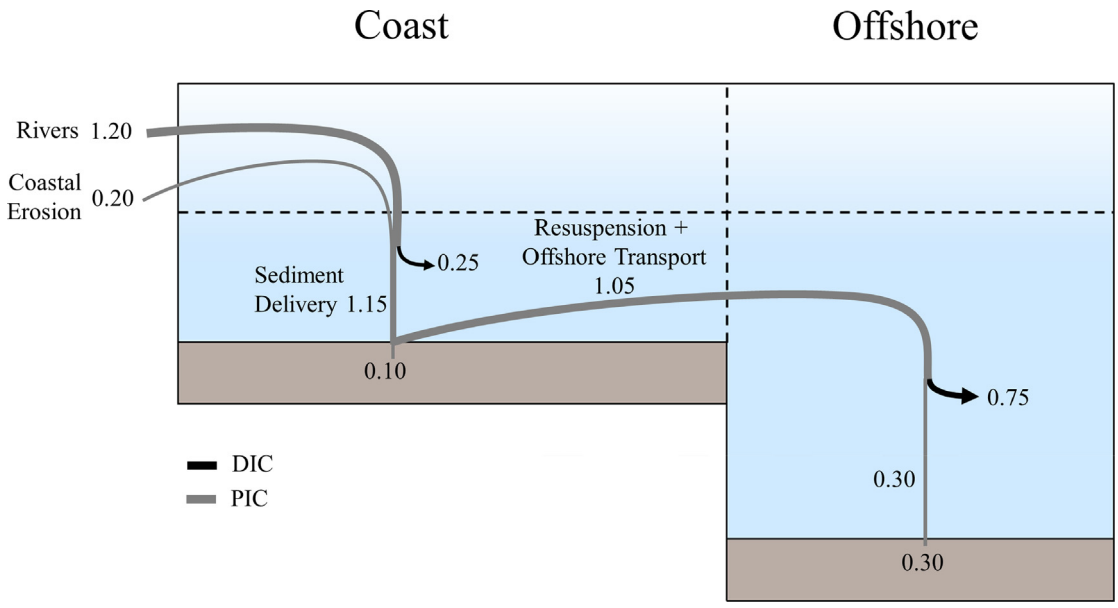

Fig. 5. Particulate inorganic carbon budget for HB. Black arrows represent DIC produced by PIC dissolution. Grey lines represent terrestrial PIC. Units are Tg C y^{-1}.

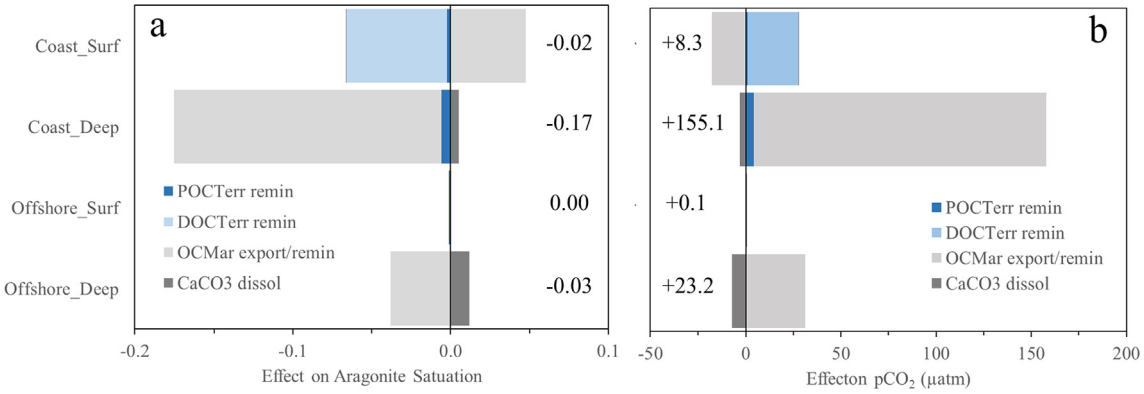

Fig. 6. Independent effects on Ω_{Ar} (panel a) and pCO_2 (panel b) of carbon cycle processes occurring within each model compartment on an annual basis. Processes include: remineralization of POC_{terr} and DOC_{terr}; production and/or remineralization of OC_{mar}; and PIC dissolution. Bar lengths represent the effect of each process on Ω_{Ar} and pCO_2. Processes that reduce Ω_{Ar} or pCO_2 are stacked on the left side of the y-axis, and processes that increase them are on the right. The net impact of C-transformations is indicated by the text label next to each bar.

remineralization, OC_{mar} production and/or remineralization, and PIC_{terr} dissolution. The bar widths represent the change in Ω_{Ar} and pCO_2 due to each process, and processes that reduce Ω_{Ar} or pCO_2 are stacked on the left side of the y-axis, while processes that increase them are on the right. In general, organic carbon remineralization increases pCO_2 accumulation and reduces Ω_{Ar}, while export production and PIC dissolution reduce pCO_2 and increase Ω_{Ar}. The net effect of all processes is equal the sum of individual effects, and is denoted by the text labels beside each bar. These values may be considered the degree to which each process alters the Ω_{Ar} state and pCO_2 of water flowing through each compartment on an annual basis, and provides an indication of the relative strength of each process. We note that the different residence times of each compartment would cause waters to be subjected to the effects of carbon transformations for different amounts of time. Although the residence times of HB waters are uncertain, it is likely that coastal surface waters have the shortest residence time while offshore deep waters have the longest.

In the coastal surface box, the mean Ω_{Ar} value is 1.23, meaning aragonite is stable in these waters on average, and is consistent with previous Ω_{Ar} measurements in HB coastal surface waters which range from 0.8 to 1.6 (Azetsu-Scott et al., 2014; Burt et al., 2016). Here, the remineralization of DOC_{terr} reduces Ω_{Ar} by 0.06 units (−5.2%), making it the largest contributor to aragonite under-saturation in this compartment. POC_{terr} remineralization had a smaller effect, reducing Ω_{Ar} by < 0.01 units, or −0.2%. These OA-promoting processes are nearly offset by the + 0.05 unit increase (+3.9%) in Ω_{Ar} from export production. The sum of these processes suggest carbon cycling lowers the Ω_{Ar} of water passing through this compartment by 0.02 units (−1.6%) on an annual basis. In the coastal deep compartment, mean Ω_{Ar} values are below saturation (0.87) consistent with previous measurements ranging from 0.6 to 1.2 (Azetsu-Scott et al., 2014; Burt et al., 2016). Here, OC_{mar} remineralization is the largest contributor to Ω_{Ar} under-saturation (−0.17 units, or −19.4%), while POC_{terr} remineralization contributes an additional decrease of 0.01units (−0.7%). These effects are moderately offset by PIC dissolution, which increases Ω_{Ar} by 0.02 units (0.6%), lowering the Ω_{Ar} of water flowing through this compartment by a total of 0.16 units per year. The Ω_{Ar} in the offshore surface compartment (mean Ω_{Ar} = 1.21) is similar to the reported range (1.0–1.7; Azetsu-Scott et al., 2014; Burt et al., 2016) and is barely affected by carbon cycling processes within the Bay, with a −0.01% effect from POC_{terr} remineralization offset by the +0.1% effect of export production. Offshore deep waters are strongly undersaturated with respect to aragonite (Ω_{Ar} = 0.83) as compared to the 0.5–1.0 reported previously (Azetsu-Scott et al., 2014; Burt et al., 2016), and are strongly influenced by OC_{mar} remineralization (-0.04 units) and PIC dissolution (+0.01 units). The residence time of water in each compartment, which is an important variable affecting the spatial distributions of Ω_{Ar}, is not accounted for by our model. The long residence times of deep waters may help explain why they are so strongly Ω_{Ar} under-saturated relative to coastal surface waters.

The impacts on pCO_2 mirrored those on Ω_{Ar}. In the coastal surface box, we estimate a mean pCO_2 of 406 µatm, or slightly super-saturated, based on the annual average temperature, salinity, DIC, TA and nutrient concentration in the compartment, consistent with net CO_2 emission estimates in coastal HB waters (340–460 µatm; Else et al., 2008a, 2008b). Here, the remineralization of DOC_{terr} increases pCO_2 by 27 µatm y^{-1} (+20%), while POC_{terr} remineralization only adds 1.0 µatm to pCO_2. Marine export production offsets this by 18 µatm (−4.4%) per year, for a net +8 µatm pCO_2 y^{-1} in this compartment. The deep coastal box has relatively high average pCO_2 (568 µatm), which is supported by a +155 µatm pCO_2 y^{-1} primarily from remineralization of OC_{mar} (+154 µatm) and POC_{terr} (+4.2 µatm), which are offset slightly by PIC dissolution (-3.1 µatm). In the offshore surface box, waters are CO_2 under-saturated (pCO_2 = 357 µatm), consistent with 280–440 µatm pCO_2 estimates by Else et al. (2008a, 2008b). Here, the very slight supply of CO_2 from POC_{terr} remineralization (+0.3 µatm pCO_2) was virtually offset by CO_2 consumed during export production (−0.2 µatm pCO_2), suggesting carbon conversions have no effect on pCO_2 in this part of HB. This implies the under-saturation observed here must be due to other factors beyond the scope of our model (e.g., carbon uptake prior to entering HB, brine rejection). Nevertheless, there is evidence for net CO_2 uptake in offshore HB waters (Else et al., 2008a, 2008b), which is consistent with pCO_2 under-saturation. In the deep offshore box, mean pCO_2 concentrations are very high (596 µatm), supported by OC_{mar} remineralization (+31 µatm pCO_2 y^{-1}) and offset slightly by PIC dissolution (−7.4 µatm pCO_2 y^{-1}). Although we did not explicitly include air-sea flux in our budget, Fig. 4 shows that the excess DIC from OC_{terr} remineralization could support up to 1.0 Tg C flux to the atmosphere as CO_2, mostly from the coastal surface box. This is somewhat lower than the 1.6 Tg mean annual CO_2 flux estimated by Else et al. (2008b), but still within a reasonable error range.

4. Discussion

From our budget (Figs. 3–5), we infer that the remineralization of POC_{terr}, DOC_{terr}, and POC_{mar} contribute to ocean acidification and CO_2 flux in HB, while export production and PIC_{terr} dissolution offset these effects to some extent. As Fig. 6 shows, POC_{terr} remineralization has a negligible impact in Hudson Bay due to the relatively small POC_{terr} inputs relative to DOC_{terr}. Although OC_{terr} remineralization makes a significant contribution to CO_2 accumulation and aragonite under-saturation in coastal surface waters, it is greatly exceeded by OC_{mar}

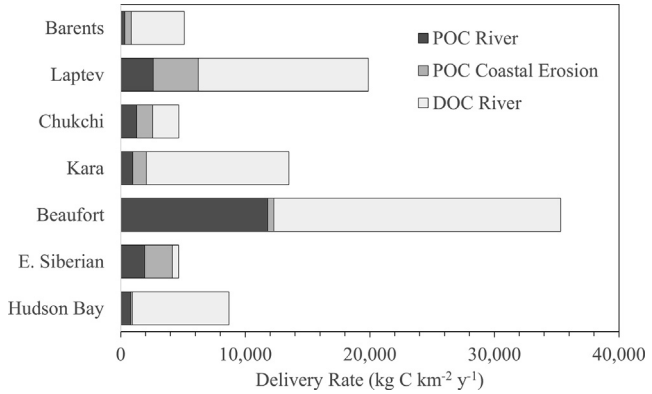

Fig. 7. Delivery rates of terrestrial organic carbon from rivers and coastal erosion to major Arctic shelf seas. Devliery rates were calculated by dividing to total annual inputs by continental shelf sea surface areas (the coastal surface area was used for Hudson Bay). See Table SI-4 for details (Stein et al., 2004; Vonk et al., 2012).

remineralization in deeper waters. Higher annual POC_{terr} inputs would make OC_{terr} remineralization a more significant driver of aragonite under-saturation and CO_2 accumulation in deep waters. Thus, the relative importance of OC_{terr} delivery depends not only on its magnitude, but also on the relative contributions from DOC and POC.

In comparison to other major Arctic shelf seas, the coastal zone of HB receives a moderate DOC_{terr} delivery rate (i.e., DOC_{terr} delivery per unit sea surface area; Fig. 7). This suggests that DOC_{terr} remineralization is likely to be a more important contributor to OA and net CO_2 evasion in other major Arctic shelf seas, particularly in the Beaufort, Kara, and Laptev Seas, which receive 1.5–3.0 × greater DOC_{terr} delivery rates than HB (see Stein and Macdonald, 2004a). The higher POC_{terr} delivery rates for other Arctic shelves (2–40 × higher than HB; except for the Barents Sea; Fig. 7) implies that POC_{terr} remineralization will be a more significant driver of OA and CO_2 for these seas. The high POC_{terr} delivery rates for the Siberian Shelves receive large contributions from coastal erosion, which is relatively minor in HB, perhaps due to high rates of isostatic rebound reducing relative sea-level rise and thus mitigating shoreline erosion. The relatively high total OC_{terr} delivery rates in shelf waters of the Laptev, Kara, Beaufort, and East Siberian Seas suggest these areas may be more vulnerable to OA and pCO_2 accumulation than HB, whereas OC_{terr} remineralization may not be as significant in the Barents and Chukchi, due to their lower total OC_{terr} delivery rates.

A key implication of the budget is that export production offsets CO_2 accumulation (70–100%) and aragonite under-saturation (65–100%) in nearshore surface waters. However, this offset strongly depends on the C:N ratios of OM_{terr}, given that export production is fueled by nutrients released during OM_{terr} remineralization. The effect of OM_{terr} remineralization decreases as the C:N ratio of OM_{terr} approaches that of OM_{mar} (i.e., 106:16). In HB, the C:N ratio of POM_{terr} is lower than DOM_{terr}, with the consequence that an increase in POM_{terr} delivery rates would not affect pCO_2 and Ω_{Ar} as much as an equal increase in DOC_{terr} delivery rates. The C:N estimates for Hudson Bay POM and DOM are similar to those observed for other major arctic rivers (Holmes et al., 2012; Mcclelland et al., 2016), suggesting that higher POC_{terr} delivery rates for other major Arctic shelf seas may not significantly increase their susceptibility to CO_2 evasion and OA, except perhaps on seasonal time-scales. Rather, the amount of DOC_{terr} they receive (and its degradability) would be the more important factors.

The budget and model also show that $CaCO_3$ dissolution offsets aragonite under-saturation in the Bay's bottom waters by 2–30%. The offsetting role of PIC dissolution appears to be more pronounced in offshore deep waters (Fig. 6). Measurements of river and coastal erosion contributions to PIC_{terr} and PIC sediment burial rates are limited both for HB and the Arctic Ocean basins (AMAP, 2013), but these sources are likely related to watershed geology with $CaCO_3$-rich basins supplying more $CaCO_3$ than silicate-dominated watersheds (Alkire et al., 2017; AMAP, 2013). The ability of $CaCO_3$ inputs to offset CO_2 produced by OC metabolism and reduce CO_2 evasion will be important for the carbonate-rich watersheds throughout the Western Canadian Arctic, including the Beaufort Sea and much of the Canadian Arctic Archipelago (Alkire et al., 2017). The potential significance of PIC to polar marine systems warrants additional research attention specifically on inputs and dissolution rates of terrestrial and marine PIC.

Its geographical location at the margin of the cryosphere places Hudson Bay in the vanguard of global climate change. Over recent decades, sea-surface temperature has increased by roughly 3 °C (Brand et al., 2014; Galbraith and Larouche, 2011), and the Bay now experiences a shorter ice-covered season (Hochheim et al., 2014; Hochheim and Barber, 2010). While warming water temperatures may accelerate microbial activity and remineralization rates (Mazuecos et al., 2015) and decrease CO_2 solubility, the shortened sea-ice season will increase wind-driven upwelling of CO_2-rich (and aragonite-under-saturated) water to the surface (Carmack and Chapman, 2003; Mathis et al., 2012), lead to greater photo-remineralization of DOC_{terr} (Bélanger et al., 2006), and facilitate exchange of CO_2 between the atmosphere and the surface ocean (AMAP, 2013; Bates, 2006). On the other hand, a prolonged open-water season would increase pelagic primary production (Arrigo et al., 2010), assuming sufficient availability of nutrients. There are many factors identified through this budget exercise that require better understanding before we can project the consequences of ongoing physical changes to the Arctic.

Hudson Bay's coasts and drainage basins contain massive peat deposits, especially along the southern coast of Hudson and James Bays where lowlands stabilized by permafrost (Gorham, 1991; Gorham et al., 2012) are undergoing thaw. Models suggest that climate warming could degrade 50% or more of this permafrost by 2050 (Gough and Leung, 2002), potentially releasing vast quantities of labile OC_{terr} to Hudson Bay (Frey and McClelland, 2009; Lawrence and Slater, 2005; Letscher et al., 2011). Recent work suggests high-latitude rivers are already becoming richer in DOC_{terr} (Monteith et al., 2007), and this will be further exacerbated by a wetter, as well as warmer, climate (De Wit et al., 2016). Variations in the volume of river discharge entering Hudson Bay occurring on decadal and multi-decadal timescales (Déry et al., 2011) will alter the rate of OM_{terr} delivery to HB. A slower delivery rate would allow more time for remineralization and CO_2 evasion within rivers, reducing the supply of labile OM_{terr} to HB, whereas higher discharge, and especially increased flooding events, would promote rapid flushing and high rates of labile OM_{terr} delivery to HB, which would promote OA. Global climate model simulations consistently project increasing pan-Arctic river discharge for the 21st century (Arnell, 2005; Holland et al., 2007; Milly et al., 2005), although in Hudson Bay both hydroelectric development and climate change will significantly impact hydrology, making it more difficult to predict future discharge trends.

We emphasize that whereas we have produced a plausible, balanced budget for both organic and inorganic carbon in HB, errors inherent in individual budget terms may significantly affect the results. We have, accordingly, performed an analysis of sensitivity to errors in our budget components. We explored the effects (Table SI-3) of variation in river discharge, the salinity of outflowing water to Hudson Strait, the nitrate concentration of upwelled waters, the DOC and POC delivery by rivers, DOC degradability, the C:N ratio of DOC_{terr}, and PIC delivery. The C:N ratio for OM_{terr} had a significant impact on Ω_{Ar} and pCO_2 in coastal surface waters. For example, lowering the C:N ratio of DOC_{terr} from 28.4 to 12.2 (the same C:N ratio as POC_{terr} in Hudson Bay) reduces the effects of OM_{terr} remineralization such that they are more than offset by export production in coastal surface waters, giving these waters a slight tendency towards CO_2 uptake from the atmosphere and increasing Ω_{Ar} values. Similarly, reducing the degradability of DOC_{terr} from 30% to

10% almost completely eliminates the tendency towards aragonite under-saturation and CO_2 accumulation in coastal surface waters. Additional uncertainty in our estimates arises from the seasonal limits of sampling in Hudson Bay, which under-represents winter and spring when sea-ice cover, river freshet, and primary production exhibit their strongest temporal gradients. Ice and benthic primary production could mitigate CO_2 accumulation and aragonite under-saturation, but little is known about their rates and distributions in HB. In summary, our sensitivity analysis indicates that better understanding of the variability in the C:N ratio and lability of terrestrial DOM is most critical to understanding future ocean acidification and the CO_2 source-sink balance of Hudson Bay, and possibly other Arctic coastal regions.

Here, we have focused our efforts directly on the components of the carbon cycle that influence CO_2 flux and ocean acidification. To these may be added sea-ice formation and melt, and river runoff, which indirectly affect the system response through driving convection (brine), reducing air-sea exchange (ice-cover, stratification), or reducing surface ocean buffer capacity (sea-ice melt, runoff). The significant freshwater inputs from both rivers and ice melt make HB particularly sensitive to ocean acidification, while brine rejection during ice formation represents a potentially significant pathway to transfer DIC from the surface to deep waters.

5. Conclusions and recommendations for future research

We have assembled here for the first time a budget that accounts for both inorganic and organic components of the carbon cycle and their interactions within Hudson Bay. To do this, we have drawn our data from numerous disparate research results published in the literature. These independent studies, most of which were conducted within the past 15 years, were not designed specifically to produce such a budget. We were therefore surprised and very much encouraged by the coherent picture these disparate data produce when quantitatively used to construct our box model (Fig. 6). Although there are clearly many uncertainties within individual components, which we have discussed, we infer that the final synthesis has a greater strength than any individual component because it incorporates so many independent parts.

Our review of existing Hudson Bay carbon studies shows that terrestrial organic carbon remineralization is an important driver of CO_2 evasion and ocean acidification, primarily in coastal surface waters. Marine primary production, on the other hand, removes CO_2 from surface water and decrease OA, but it does so by adding to these in deep waters. Overall, carbon cycling within the Bay promotes aragonite under-saturation and increasing pCO_2 everywhere except in offshore surface waters, with the largest impacts in deep coastal waters. Seawater entering Hudson Bay is already in a state of low pH/high CO_2 (Azetsu-Scott et al., 2010); these waters are further modified within Hudson Bay, which, in consequence, contribute corrosive water to Hudson Strait and the Labrador Sea.

The effects of OM_{terr} remineralization in coastal surface waters are significantly offset by export production and $CaCO_3$ dissolution. Since export production is partially fuelled by nutrients released during OM_{terr} remineralization, the offset inherent in OM_{terr} depends strongly on its C:N ratio, which is higher for DOM_{terr} relative to POM_{terr} (Table 1). Furthermore, the lability of OM is related to its C:N ratio; DOM_{terr} is least labile (C:N = 28.6, 30% remineralized), followed by POM_{terr} (C:N = 8.2, ~60% remineralized), and POM_{mar} (C:N = 6.6, > 95% remineralized). The dissolution of terrestrial $CaCO_3$ also counters the effects of OC remineralization on pCO_2 and OA, but this is likely restricted to deep waters where $CaCO_3$ is under-saturated.

Hydrological change (damming/diversion) and climate change over the past century have already altered the Hudson Bay's fresh water and carbon cycle, with more pronounced changes projected for the next century. Our synthesis implies that ocean acidification will increase in Hudson Bay, and time-series studies should be put in place to follow its progress. Greater research emphasis needs to be placed especially on spring and autumn freeze-up. River geochemistry is particularly undersampled during freshet, despite the importance of this time period for carbon transport. The contribution of ice-algae, macroalgae, seagrasses, and benthos to the Bay's primary productivity remains a glaring data gap, despite its likely importance to remove CO_2 (e.g., see Glud et al., 2009) and therefore modify pH, pCO_2, and Ω (Duarte et al., 2013). Permafrost in the southern Hudson Bay and James Bay Lowlands contains large inventories of OM_{terr} at risk from thaw, and old permafrost carbon is already being released (AMAP, 2017; Feng et al., 2013). There is evidence that ancient carbon is being mobilized as DOC in some Hudson Bay river basins (Godin et al., 2017). Further investigation of the age and composition of OC_{terr} entering HB is needed to determine the present rate of supply of ancient OC to the Bay and set a baseline against which to measure change.

Our findings imply that higher OC_{terr} delivery rates in other major Arctic shelf seas, especially POC_{terr}, may promote more intense rates of CO_2 efflux and acidification relative to HB, especially if POC_{terr} is remineralized under light-limitation when primary production is suppressed. Like Hudson Bay, the C:N ratios of OM_{terr} entering the Arctic Ocean and its degradability, as well as the supply and dissolution of terrestrial $CaCO_3$ need greater sampling emphasis.

Declaration of Competing Interest

The authors declare that they have no known competing financial interests or personal relationships that could have appeared to influence the work reported in this paper.

Acknowledgements

We wish to acknowledge all the individuals whose efforts contributed to the data that made this work possible. This work was conducted as part of the ArcticNet and Baysys Research projects with funding from the contributions of the Natural Sciences and Engineering Research Council (NSERC), Manitoba Hydro, and the University of Manitoba. All data are available from authors. We acknowledge the contributions from both NSERC's Discovery and Collaborative Research and Development Programs, and the Networks of Centres of Excellence Program. We are grateful for the reviewers who provided encouragement and helpful comments in review.

Appendix A. Supplementary material

Supplementary data to this article can be found online at https://doi.org/10.1016/j.pocean.2020.102319.

References

Alkire, M.B., Jacobson, A.D., Lehn, G.O., Macdonald, R.W., Rossi, M.W., 2017. On the geochemical heterogeneit of rivers draining into the straits and channels of the Canadian Arctic Archipelago. J. Geophys. Res. Biogeosci. 122, 2527–2547. https://doi.org/10.1002/2016JG003723.

AMAP, 2017. Snow, water, ice and parmafrost in the Arctic (SWIPA) 2017. Arctic Monitoring and Assessment Programme (AMAP), Oslo, Norway. xiv + 269 pp.

AMAP, 2013. AMAP assessment 2013: Arctic Ocean Acidification. Arctic Monitoring and Assessment Programme (AMAP), Amap, 2013. Oslo, Norway viii + 99pp.

Amon, R.M.W., 2004. The role of dissolved organic matter for the organic carbon cycle in the Arctic Ocean. In: The Organic Carbon Cycle in the Arctic Ocean. Springer, Berlin, Heidelberg, Berlin, Heidelberg, pp. 83–99. https://doi.org/10.1007/978-3-642-18912-8_4.

Anderson, J.T., Roff, J.C., 1980. Seston ecology of the surface waters of Hudson Bay. Can. J. Fish. Aquat. Sci. 37, 2242–2253. https://doi.org/10.1139/f80-269.

Arnell, N.W., 2005. Implications of climate change for freshwater inflows to the Arctic Ocean. J. Geophys. Res. Atmos. 110, 1–9. https://doi.org/10.1029/2004JD005348.

Arrigo, K.R., Pabi, S., van Dijken, G.L., Maslowski, W., 2010. Air-sea flux of CO_2 in the Arctic Ocean, 1998–2003. J. Geophys. Res. 115, G04024. https://doi.org/10.1029/2009JG001224.

Azetsu-Scott, K., Clarke, A., Falkner, K., Hamilton, J., Jones, E.P., Lee, C., Petrie, B., Prinsenberg, S., Starr, M., Yeats, P., 2010. Calcium carbonate saturation states in the waters of the Canadian Arctic Archipelago and the Labrador Sea. J. Geophys. Res. 115, C11021. https://doi.org/10.1029/2009JC005917.

Azetsu-Scott, K., Starr, M., Mei, Z.-P., Granskog, M., 2014. Low calcium carbonate saturation state in an Arctic inland sea having large and varying fluvial inputs: the Hudson Bay system. J. Geophys. Res. Ocean. 119, 6210–6220. https://doi.org/10.1002/2014JC009948.

Azevedo, L.B., Schryver, A.M. De, Hendriks, A.J., Huijbregts, M.A.J., 2015. Calcifying species sensitivity distributions for ocean acidification. Environ. Sci. Technol. 49, 1495–1500. https://doi.org/10.1021/es505485m.

Baker, R.F., 1989. An environmental assessment and biological investigation of the Nelson River estuary, Report prepared for Manitoba Hydro. North/South Consultants Inc., Winnipeg, p. 179.

Bates, N.R., 2006. Air-sea CO_2 fluxes and the continental shelf pump of carbon in the Chukchi Sea adjacent to the Arctic Ocean. J. Geophys. Res. Ocean. 111, 1–21. https://doi.org/10.1029/2005JC003083.

Bauer, J.E., Bianchi, T.S., 2012. Dissolved Organic Carbon Cycling and Transformation, Treatise on Estuarine and Coastal Science. Elsevier Inc. https://doi.org/10.1016/B978-0-12-374711-2.00502-7.

Bélanger, S., Xie, H., Krotkov, N., Larouche, P., Vincent, W.F., Babin, M., 2006. Photomineralization of terrigenous dissolved organic matter in arctic coastal waters from 1979 to 2003: interannual variability and implications of climate change. Global Biogeochem. Cycles 20, 1–13. https://doi.org/10.1029/2006GB02708.

Bianchi, T.S., 2011. The role of terrestrially derived organic carbon in the coastal ocean: a changing paradigm and the priming effect. Proc. Natl. Acad. Sci. 108, 19473–19481. https://doi.org/10.1073/pnas.1017982108.

Brand, U., Came, R.E., Affek, H., Azmy, K., Mooi, R., Layton, K., 2014. Climate-forced change in Hudson Bay seawater composition and temperature, Arctic Canada. Chem. Geol. 388, 78–86. https://doi.org/10.1016/j.chemgeo.2014.08.028.

Brown, K.A., Miller, L.A., Mundy, C.J., Papakyriakou, T., Francois, R., Gosselin, M., Carnat, G., Swystun, K., Tortell, P.D., 2015. Inorganic carbon system dynamics in landfast Arctic sea ice during the early-melt period. J. Geophys. Res. Ocean. 120, 3542–3566. https://doi.org/10.1002/2014JC010620.

Burt, W.J., Thomas, H., Miller, L.A., Granskog, M.A., Papakyriakou, T.N., Pengelly, L., 2016. Inorganic carbon cycling and biogeochemical processes in an Arctic inland sea (Hudson Bay). Biogeosciences 13, 4659–4671. https://doi.org/10.5194/bg-13-4659-2016.

Caldeira, K., Wickett, M.E., 2003. Anthropogenic carbon and ocean pH. Nature 425, 365 365. https://doi.org/10.1038/425365a.

Carmack, E., Chapman, D.C., 2003. Wind-driven shelf/basin exchange on an Arctic shelf: the joint roles of ice cover extent and shelf-break bathymetry. Geophys. Res. Lett. 30, 3–6. https://doi.org/10.1029/2003GL017526.

Carmack, E.C., Yamamoto-Kawai, M., Haine, T.W.N., Bacon, S., Bluhm, B.A., Lique, C., Melling, H., Polyakov, I.V., Straneo, F., Timmermans, M.L., Williams, W.J., 2016. Freshwater and its role in the Arctic Marine System: Sources, disposition, storage, export, and physical and biogeochemical consequences in the Arctic and global oceans. J. Geophys. Res. G Biogeosci. 121, 675–717. https://doi.org/10.1002/2015JG003140.

Catalá, T.S., Reche, I., Fuentes-Lema, A., Romera-Castillo, C., Nieto-Cid, M., Ortega-Retuerta, E., Calvo, E., Álvarez, M., Marrasé, C., Stedmon, C.A., Álvarez-Salgado, X.A., 2015. Turnover time of fluorescent dissolved organic matter in the dark global ocean. Nat. Commun. 6. https://doi.org/10.1038/ncomms6986.

Ciais, P., Sabine, C., Bala, G., Bopp, L., Brovkin, V., Canadell, J., Chhabra, A., DeFries, R., Galloway, J., Heimann, M., Jones, C., Le Quéré, C., Myneny, R.B., Piao, S., Thornton, P., 2013. Carbon and Other Biogeochemical Cycles Chapter 6. Clim. Chang. 2013 Phys. Sci. Basis. Contrib. Work. Gr. I to Fifth Assess. Rep. Intergov. Panel Clim. Chang., pp. 465–570. https://doi.org/10.1017/CBO9781107415324.014.

CliC/AMAP/IASC, 2016. The Arctic Freshwater System in a Changing Climate. WCRP Clim. Cryosph. Proj. Arct. Monit. Assess. Program. (AMAP), Int. Arct. Sci. Comm. (IASC).

Cota, G.F., Legendre, L., Gosselin, M., Ingram, R.G., 1991. Ecology of bottom ice algae: I. Environmental controls and variability. J. Mar. Syst. 2, 257–277. https://doi.org/10.1016/0924-7963(91)90036-T.

Couture, N.J., Irrgang, A., Pollard, W., Lantuit, H., Fritz, M., 2018. Coastal erosion of permafrost soils along the Yukon Coastal plain and fluxes of organic carbon to the Canadian Beaufort Sea. J. Geophys. Res. Biogeosci. 123, 406–422. https://doi.org/10.1002/2017JG004166.

Dai, A., Qian, T., Trenberth, K.E., Milliman, J.D., 2009. Changes in continental freshwater discharge from 1948 to 2004. J. Clim. 22, 2773–2792. https://doi.org/10.1175/2008JCLI2592.1.

Dainard, P.G., Guéguen, C., McDonald, N., Williams, W.J., 2015. Photobleaching of fluorescent dissolved organic matter in Beaufort Sea and North Atlantic Subtropical Gyre. Mar. Chem. 177, 630–637. https://doi.org/10.1016/j.marchem.2015.10.004.

De Wit, H.A., Valinia, S., Weyhenmeyer, G.A., Futter, M.N., Kortelainen, P., Austnes, K., Hessen, D.O., Räike, A., Laudon, H., Vuorenmaa, J., 2016. Current browning of surface waters will be further promoted by wetter climate. Environ. Sci. Technol. Lett. 3, 430–435. https://doi.org/10.1021/acs.estlett.6b00396.

Denfeld, B., Frey, K., Sobczak, W., 2013. Summer CO_2 evasion from streams and rivers in the Kolyma River basin, north-east Siberia. Polar 1, 1–15. https://doi.org/10.3402/polar.v32i0.19704.

Déry, S.J., Mlynowski, T.J., Hernández-Henríquez, M.A., Straneo, F., 2011. Interannual variability and interdecadal trends in Hudson Bay Streamflow. J. Mar. Syst. 88, 341–351. https://doi.org/10.1016/j.jmarsys.2010.12.002.

Déry, S.J., Stadnyk, T.A., MacDonald, M.K., Gauli-Sharma, B., 2016. Recent trends and variability in river discharge across northern Canada. Hydrol. Earth Syst. Sci. 20, 4801–4818. https://doi.org/10.5194/hess-20-4801-2016.

Dieckmann, G.S., Nehrke, G., Uhlig, C., Göttlicher, J., Gerland, S., Granskog, M.A., Thomas, D.N., 2010. Brief Communication: Ikaite ($CaCO_3{\cdot}6H_2O$) discovered in Arctic sea ice. Cryosph. 4, 227–230. https://doi.org/10.5194/tc-4-227-2010.

Doney, S.C., Fabry, V.J., Feely, R.A., Kleypas, J.A., 2009. Ocean acidification: the Other CO_2 problem. Ann. Rev. Mar. Sci. 1, 169–192. https://doi.org/10.1146/annurev.marine.010908.163834.

Duarte, C.M., Hendriks, I.E., Moore, T.S., Olsen, Y.S., Steckbauer, A., Ramajo, L., Carstensen, J., Trotter, J.A., McCulloch, M., 2013. Is ocean acidification an open-ocean syndrome? Understanding anthropogenic impacts on seawater pH. Estuaries and Coasts 36, 221–236. https://doi.org/10.1007/s12237-013-9594-3.

Dunbar, M.J., 1993. Hudson Bay has too much fresh water. 4(2), Report for the Center for Climate and Global Change Research - McGill University, Montreal, Canada, pp. 12-13.

Else, B.G.T., Galley, R.J., Papakyriakou, T.N., Miller, L.A., Mucci, A., Barber, D., 2012. Sea surface pCO_2 cycles and CO_2 fluxes at landfast sea ice edges in Amundsen Gulf, Canada. J. Geophys. Res. 117 (12), C09010. https://doi.org/10.1029/2012JC007901.

Else, B.G.T., Papakyriakou, T.N., Granskog, M.A., Yackel, J.J., 2008a. Observations of sea surface fCO_2 distributions and estimated air-sea CO_2 fluxes in the Hudson Bay region (Canada) during the open water season. J. Geophys. Res. 113, 1–12. https://doi.org/10.1029/2007JC004389.

Else, B.G.T., Yackel, J.J., Papakyriakou, T.N., 2008b. Application of satellite remote sensing techniques for estimating air – sea CO_2 fluxes in Hudson Bay, Canada during the ice-free season. Remote Sens. Environ. 112, 3550–3562. https://doi.org/10.1016/j.rse.2008.04.013.

Eppley, R.W., Peterson, B.J., 1979. Particulate organic matter flux and planktonic new production in the deep ocean. Nature 282, 677–680. https://doi.org/10.1038/282677a0.

Feng, X., Vonk, J.E., van Dongen, B.E., Gustafsson, O., Semiletov, I.P., Dudarev, O.V., Wang, Z., Montlucon, D.B., Wacker, L., Eglinton, T.I., 2013. Differential mobilization of terrestrial carbon pools in Eurasian Arctic river basins. Proc. Natl. Acad. Sci. 110, 14168–14173. https://doi.org/10.1073/pnas.1307031110.

Ferland, J., Gosselin, M., Starr, M., 2011. Environmental control of summer primary production in the Hudson Bay system: the role of stratification. J. Mar. Syst. 88, 385–400. https://doi.org/10.1016/j.jmarsys.2011.03.015.

Frey, K.E., McClelland, J.W., 2009. Impacts of permafrost degradation on arctic river biogeochemistry. Hydrol. Process. 23, 169–182. https://doi.org/10.1002/hyp.7196.

Galbraith, P.S., Larouche, P., 2011. Sea-surface temperature in Hudson Bay and Hudson Strait in relation to air temperature and ice cover breakup, 1985–2009. J. Mar. Syst. 87, 66–78. https://doi.org/10.1016/j.jmarsys.2011.06.006.

Geilfus, N.-X., Tison, J.-L., Ackley, S.F., Galley, R.J., Rysgaard, S., Miller, L.A., Delille, B., 2014. Sea ice pCO_2 dynamics and air–ice CO_2 fluxes during the Sea Ice Mass Balance in the Antarctic (SIMBA) experiment – Bellingshausen Sea, Antarctica. Cryosph. 8, 2395–2407. https://doi.org/10.5194/tc-8-2395-2014.

Glud, R.N., Woelfel, J., Karsten, U., Kühl, M., Rysgaard, S., 2009. Benthic microalgal production in the Arctic: applied methods and status of the current database. Bot. Mar. 52, 559–571. https://doi.org/10.1515/BOT.2009.074.

Godin, P., Macdonald, R.W., Kuzyk, Z.A., Goñi, M.A., Stern, G.A., 2017. Organic matter compositions of rivers draining into Hudson Bay: present-day trends and potential as recorders of future climate change. J. Geophys. Res. Biogeosci. 122, 1848–1869. https://doi.org/10.1002/2016JG003569.

Gordon, D., Boudreau, P., Mann, K., Ong, W., Silvert, S., Smith, G., Wattayakorn, G., Wulff, F., Yanagi, T., 1996. LOICZ Biogeochemical Modelling Guidelines. LOICZ/R&S/95-5, VI, 96 pp. LOICZ, TEXEL, Netherlands.

Gorham, E., 1991. Northern Peatlands: Role in the Carbon Cycle and Probable Responses to Climatic Warming. Ecol. Appl. 1, 182–195. https://doi.org/10.2307/1941811. (in press).

Gorham, E., Lehman, C., Dyke, A., Clymo, D., Janssens, J., 2012. Long-term carbon sequestration in North American peatlands. Quat. Sci. Rev. 58, 77–82. https://doi.org/10.1016/j.quascirev.2012.09.018. (in press).

Gough, W., Leung, A., 2002. Nature and fate of Hudson Bay permafrost. Reg. Environ. Chang. 2, 177–184. https://doi.org/10.1007/s10113-002-0048-x.

Granskog, M.A., Kuzyk, Z.A., Azetsu-Scott, K., Macdonald, R.W., 2011. Distributions of runoff, sea-ice melt and brine using $\delta^{18}O$ and salinity data — a new view on freshwater cycling in Hudson Bay. J. Mar. Syst. 88, 362–374. https://doi.org/10.1016/j.jmarsys.2011.03.011.

Granskog, M.A., Macdonald, R.W., Kuzyk, Z.A., Senneville, S., Mundy, C.-J., Barber, D.G., Stern, G.A., Saucier, F., 2009. Coastal conduit in southwestern Hudson Bay (Canada) in summer: rapid transit of freshwater and significant loss of colored dissolved organic matter. J. Geophys. Res. 114, 1–15. https://doi.org/10.1029/2009JC005270.

Granskog, M.A., Macdonald, R.W., Mundy, C.-J., Barber, D.G., 2007. Distribution, characteristics and potential impacts of chromophoric dissolved organic matter (CDOM) in Hudson Strait and Hudson Bay, Canada. Cont. Shelf Res. 27, 2032–2050. https://doi.org/10.1016/j.csr.2007.05.001.

Griffiths, J.L., 2010. Microfossil Evidence for Recent and Past Changes to Hudson Bay Oceanography. M.Sc. Thesis. Dalhousie Univ. Halifax.

Guéguen, C., Cuss, C.W., Cassels, C.J., Carmack, E.C., 2014. Absorption and fluorescence of dissolved organic matter in the waters of the Canadian Artic Archiipelago, Baffin Bay, and the Labrador Sea. J. Geophys. Res. Ocean. 119, 2034–2047. https://doi.org/10.1002/2013JC009173.Received.

Guéguen, C., Granskog, M.A., McCullough, G., Barber, D.G., 2011. Characterisation of colored dissolved organic matter in Hudson Bay and Hudson Strait using parallel factor analysis. J. Mar. Syst. 88, 423–433. https://doi.org/10.1016/j.jmarsys.2010.12.001.

Guéguen, C., Mokhtar, M., Perroud, A., McCullough, G., Papakyriakou, T., 2016. Mixing and photoreactivity of dissolved organic matter in the Nelson/Hayes estuarine system (Hudson Bay, Canada). J. Mar. Syst. 161, 42–48. https://doi.org/10.1016/j.jmarsys.2016.05.005.

Hansell, D.A., 2013. Recalcitrant dissolved organic carbon fractions. Ann. Rev. Mar. Sci.

5, 421–445. https://doi.org/10.1146/annurev-marine-120710-100757.
Heikkilä, M., Pospelova, V., Forest, A., Stern, G.A., Fortier, L., Macdonald, R.W., 2016. Dinoflagellate cyst production over an annual cycle in seasonally ice-covered Hudson Bay. Mar. Micropaleontol. 125, 1–24. https://doi.org/10.1016/j.marmicro.2016.02.005.
Heikkilä, M., Pospelova, V., Hochheim, K.P., Kuzyk, Z.A., Stern, G.A., Barber, D.G., Macdonald, R.W., 2014. Surface sediment dinoflagellate cysts from the Hudson Bay system and their relation to freshwater and nutrient cycling. Mar. Micropaleontol. 106, 79–109. https://doi.org/10.1016/j.marmicro.2013.12.002.
Herlemann, D.P.R., Manecki, M., Meeske, C., Pollehne, F., Labrenz, M., Schulz-Bull, D., Dittmar, T., Jürgens, K., 2014. Uncoupling of bacterial and terrigenous dissolved organic matter dynamics in decomposition experiments. PLoS One 9, e93945. https://doi.org/10.1371/journal.pone.0093945.
Hillaire-Marcel, C., Fairbridge, R.W., 1978. Isostasy and eustasy of Hudson Bay. Geology 6, 117–122. https://doi.org/10.1130/0091-7613(1978)6<117:IAEOHB>2.0.CO;2.
Hochheim, K.P., Barber, D.G., 2010. Atmospheric forcing of sea ice in Hudson Bay during the fall period, 1980–2005. J. Geophys. Res. 115, C05009. https://doi.org/10.1029/2009JC005334.
Hochheim, K.P., Barber, D.G., Barber, D.G., 2014. An update on the ice climatology of the Hudson Bay system an update on the ice climatology of the Hudson Bay System. Arctic. Antarct. Alp. Res. 46, 66–83.
Holding, J.M., Duarte, C.M., Delgado-Huertas, A., Soetaert, K., Vonk, J.E., Agustí, S., Wassmann, P., Middelburg, J.J., 2017. Autochthonous and allochthonous contributions of organic carbon to microbial food webs in Svalbard fjords. Limnol. Oceanogr. 62, 1307–1323. https://doi.org/10.1002/lno.10526.
Holland, M.M., Finnis, J., Barrett, A.P., Serreze, M.C., 2007. Projected changes in Arctic Ocean freshwater budgets. J. Geophys. Res. Biogeosci. 112, 1–13. https://doi.org/10.1029/2006JG000354.
Holmes, R.M., McClelland, J.W., Peterson, B.J., Tank, S.E., Bulygina, E., Eglinton, T.I., Gordeev, V.V., Gurtovaya, T.Y., Raymond, P.A., Repeta, D.J., Staples, R., Striegl, R.G., Zhulidov, A.V., Zimov, S.A., 2012. Seasonal and annual fluxes of nutrients and organic matter from large rivers to the Arctic Ocean and surrounding seas. Estuaries and Coasts 35, 369–382. https://doi.org/10.1007/s12237-011-9386-6.
Holmes, R.M., McClelland, J.W., Raymond, P.A., Frazer, B.B., Peterson, B.J., Stieglitz, M., 2008. Lability of DOC transported by Alaskan rivers to the Arctic Ocean. Geophys. Res. Lett. 35, 3–7. https://doi.org/10.1029/2007GL032837.
Kaltin, S., Anderson, L.G., 2005. Uptake of atmospheric carbon dioxide in Arctic shelf seas: evaluation of the relative importance of processes that influence pCO_2 in water transported over the Bering-Chukchi Sea shelf. Mar. Chem. 94, 67–79. https://doi.org/10.1016/j.marchem.2004.07.010.
Kawahigashi, M., Kaiser, K., Kalbitz, K., Rodionov, A., Guggenberger, G., 2004. Dissolved organic matter in small streams along a gradient from discontinuous to continuous permafrost. Glob. Chang. Biol. 10, 1576–1586. https://doi.org/10.1111/j.1365-2486.2004.00827.x.
Kirk, J.L., Louis, V.L.S., 2009. Multiyear total and methyl mercury exports from two major sub-arctic rivers draining into Hudson Bay, Canada. Environ. Sci. Technol. 43, 2254–2261. https://doi.org/10.1021/es803138z.
König, D., Miller, L.A., Simpson, K.G., Vagle, S., 2018. Carbon dynamics during the formation of sea ice at different growth rates. Front. Earth Sci. 6, 234. https://doi.org/10.3389/feart.2018.00234.
Kuzyk, Z.A., Goñi, M.A., Stern, G.A., Macdonald, R.W., 2008. Sources, pathways and sinks of particulate organic matter in Hudson Bay: evidence from lignin distributions. Mar. Chem. 112, 215–229. https://doi.org/10.1016/j.marchem.2008.08.001.
Kuzyk, Z.A., Macdonald, R.W., Johannessen, S.C., Gobeil, C., Stern, G.A., 2009. Towards a sediment and organic carbon budget for Hudson Bay. Mar. Geol. 264, 190–208. https://doi.org/10.1016/j.margeo.2009.05.006.
Kuzyk, Z.A., Macdonald, R.W., Tremblay, J.É., Stern, G.A., 2010. Elemental and stable isotopic constraints on river influence and patterns of nitrogen cycling and biological productivity in Hudson Bay. Cont. Shelf Res. 30, 163–176. https://doi.org/10.1016/j.csr.2009.10.014.
Kwok, R., Cunningham, G.F., Wensnahan, M., Rigor, I., Zwally, H.J., Yi, D., 2009. Thinning and volume loss of the Arctic Ocean sea ice cover: 2003–2008. J. Geophys. Res. Ocean. 114, 2003–2008. https://doi.org/10.1029/2009JC005312.
Lalumière, R., Messier, D., Fournier, J.-J., McRoy, C.P., 1994. Eelgrass meadows in a low arctic environment, the northeast coast of James Bay, Québec. Aquat. Bot. 47, 303–315. https://doi.org/10.1016/0304-3770(94)90060-4.
Lantuit, H., Overduin, P.P., Couture, N., Wetterich, S., Aré, F., Atkinson, D., Brown, J., Cherkashov, G., Drozdov, D., Forbes, D.L., Graves-Gaylord, A., Grigoriev, M., Hubberten, H., Jordan, J., Jorgenson, T., Ødegård, R.S., Ogorodov, S., Pollard, W.H., Rachold, V., Sedenko, S., Solomon, S., Steenhuisen, F., Streletskaya, I., Vasiliev, A., 2012. The Arctic Coastal Dynamics Database: a new classification scheme and statistics on arctic permafrost coastlines. Estuaries and Coasts 35, 383–400. https://doi.org/10.1007/s12237-010-9362-6.
Lapoussière, A., Michel, C., Gosselin, M., Poulin, M., 2009. Spatial variability in organic material sinking export in the Hudson Bay system, Canada, during fall. Cont. Shelf Res. 29, 1276–1288. https://doi.org/10.1016/j.csr.2009.02.004.
Lapoussière, A., Michel, C., Gosselin, M., Poulin, M., Martin, J., Tremblay, J.-É., 2013. Primary production and sinking export during fall in the Hudson Bay system, Canada. Cont. Shelf Res. 52, 62–72. https://doi.org/10.1016/j.csr.2012.10.013.
Lawrence, D.M., Slater, A.G., 2005. A projection of severe near-surface permafrost degradation during the 21st century. Geophys. Res. Lett. 32, 1–5. https://doi.org/10.1029/2005GL025080.
Letscher, R.T., Hansell, D.A., Kadko, D., 2011. Rapid removal of terrigenous dissolved organic carbon over the Eurasian shelves of the Arctic Ocean. Mar. Chem. 123, 78–87. https://doi.org/10.1016/j.marchem.2010.10.002.
Loladze, I., Elser, J.J., 2011. The origins of the Redfield nitrogen-to-phosphorus ratio are in a homoeostatic protein-to-rRNA ratio. Ecol. Lett. 14, 244–250. https://doi.org/10.1111/j.1461-0248.2010.01577.x.
Manizza, M., Follows, M.J., Dutkiewicz, S., Menemenlis, D., Hill, C.N., Key, R.M., 2013. Changes in the Arctic Ocean CO_2 sink (1996–2007): a regional model analysis. Global Biogeochem. Cycles 27, 1108–1118. https://doi.org/10.1002/2012GB004491.
Mann, P.J., Davydova, A., Zimov, N., Spencer, R.G.M., Davydov, S., Bulygina, E., Zimov, S., Holmes, R.M., 2012. Controls on the composition and lability of dissolved organic matter in Siberia's Kolyma River basin. J. Geophys. Res. Biogeosci. 117, 1–15. https://doi.org/10.1029/2011JG001798.
Mathis, J.T., Pickart, R.S., Byrne, R.H., McNeil, C.L., Moore, G.W.K., Juranek, L.W., Liu, X., Ma, J., Easley, R.A., Elliot, M.M., Cross, J.N., Reisdorph, S.C., Bahr, F., Morison, J., Lichendorf, T., Feely, R.A., 2012. Storm-induced upwelling of high pCO2 waters onto the continental shelf of the western Arctic Ocean and implications for carbonate mineral saturation states. Geophys. Res. Lett. 39, 1–7. https://doi.org/10.1029/2012GL051574.
Mazuecos, I.P., Arístegui, J., Vázquez-domínguez, E., Ortega-retuerta, E., Gasol, J.M., Reche, I., 2015. Temperature control of microbial respiration and growth efficiency in the mesopelagic zone of the South Atlantic and Indian Oceans. Deep. Res. Part I 95, 131–138. https://doi.org/10.1016/j.dsr.2014.10.014.
McClelland, J.W., Holmes, R.M., Dunton, K.H., Macdonald, R.W., 2012. The Arctic Ocean Estuary. Estuaries and Coasts 35, 353–368. https://doi.org/10.1007/s12237-010-9357-3.
Mcclelland, J.W., Holmes, R.M., Peterson, B.J., Raymond, P.A., Striegl, R.G., Zhulidov, A.V., Zimov, S.A., Zimov, N., Tank, S.E., Spencer, R.G.M., Staples, R., Gurtovaya, T.Y., Griffin, C.G., 2016. Particulate organic carbon and nitrogen export from major Arctic rivers. Global Biogeochem. Cycles 30, 629–643. https://doi.org/10.1002/2015GB005351.
McCullough, G., Kuzyk, Z.A., Ehn, J., Babb, D.G., Ridenour, N., Myers, P.G., Wong, K., Koenig, K., Sydor, K., Barber, D.G., 2019. Freshwater-marine interactions inthe Greater Hudson Bay Marine Region. In: Kuzyk, Z.A., Candlish, L.M. (Eds.), From Science to Policy in the Greater Hudson Bay Marine Region: An Integrated Regional Impact Study. (IRIS) of Climate Change and Modernization.
Messier, D., Ingram, R.G., Roy, D., 1986. Physical and ibological modifications in response to La Grande hydroelectric complex. In: Martini, I.P. (Ed.), Canadian Inland Seas. Elsevier, Amsterdam, pp. 403–424 (in press).
Milly, P.C.D., Dunne, A.K., Vecchia, A.V., 2005. Global pattern of trends in streamflow and water availability in a changing climate. Nature 438, 347–350.
Monteith, D.T., Stoddard, J.L., Evans, C.D., De Wit, H.A., Forsius, M., Høgåsen, T., Wilander, A., Skjelkvåle, B.L., Jeffries, D.S., Vuorenmaa, J., Keller, B., Kopécek, J., Vesely, J., 2007. Dissolved organic carbon trends resulting from changes in atmospheric deposition chemistry. Nature 450, 537–540. https://doi.org/10.1038/nature06316.
Moreau, S., Vancoppenolle, M., Bopp, L., Aumont, O., Madec, G., Delille, B., Tison, J.-L., Barriat, P.-Y., Goosse, H., 2016. Assessment of the sea-ice carbon pump: Insights from a three-dimensional ocean-sea-ice-biogeochemical model (NEMO-LIM-PISCES). Elem. Sci. Anthr. 4, 1–14. https://doi.org/10.12952/journal.elementa.000136.
Mundy, C.J., Gosselin, M., Starr, M., Michel, C., 2010. Riverine export and the effects of circulation on dissolved organic carbon in the Hudson Bay system. Canada. Limnol. Oceanogr. 55, 315–323. https://doi.org/10.4319/lo.2010.55.1.0315.
Östlund, H.G., Possnert, G., Swift, J.H., 1987. Ventilation rate of the deep Arctic Ocean from carbon 14 data. J. Geophys. Res. Ocean 92, 3769–3777.
Pegau, W.S., 2002. Inherent optical properties of the central Arctic surface waters. J. Geophys. Res. 107, 8035. https://doi.org/10.1029/2000JC000382.
Pierrot, D.E.L., Wallace, D.W.R., 2006. MS Excel Program Developed for CO_2 System Calculations. ORNL/CDIAC-105a. Carbon Dioxide Information Analysis Center, Oak Ridge National Laboratory, U.S. Department of Energy, Oak Ridge, Tennessee.
Raymond, P.A., Bauer, J.E., 2000. Bacterial consumption of DOC during transport through a temperate estuary. Aquat. Microb. Ecol. 22, 1–12.
Redfield, A., 1934. On the proportions of organic derivatives in sea water and their relation to the composition of plankton. Daniel, R.J. (Ed.), JAmes Johnstone Meml. Vol. Univ. Press Liverpool, pp. 177–192.
Retelletti Brogi, S., Ha, S.Y., Kim, K., Derrien, M., Lee, Y.K., Hur, J., 2018. Optical and molecular characterization of dissolved organic matter (DOM) in the Arctic ice core and the underlying seawater (Cambridge Bay, Canada): implication for increased autochthonous DOM during ice melting. Sci. Total Environ. 627, 802–811. https://doi.org/10.1016/j.scitotenv.2018.01.251.
Roff, J.C., Legendre, L., 1986. Physico-chemical and biological oceanography of Hudson Bay., in. In: Martini, I.P. (Ed.), Canadian Inland Seas. Elsevier, New York, pp. 265–291.
Rosa, E., Gaillardet, J., Hillaire-Marcel, C., Hélie, J.-F., Richard, L.-F., 2012. Rock denudation rates and organic carbon exports along a latitudinal gradient in the Hudson, James, and Ungava bays watershed. Can. J. Earth Sci. 49, 742–757. https://doi.org/10.1139/e2012-021.
Rysgaard, S., Bendtsen, J., Delille, B., Dieckmann, G.S., Glud, R.N., Kennedy, H., Mortensen, J., Papadimitriou, S., Thomas, D.N., Tison, J.-L., 2011. Sea ice contribution to the air–sea CO_2 exchange in the Arctic and Southern Oceans. Tellus B Chem. Phys. Meteorol. 63, 823–830. https://doi.org/10.1111/j.1600-0889.2011.00571.x.
Sarmiento, J.L., Gruber, N., 2006. Carbon Cycle. In: Ocean Biogeochemical Dynamics. Princeton University Press, Princeton, New Jersey, pp. 318–358.
Saucier, F.J., Senneville, S., Prinsenberg, S.J., Roy, F., Smith, G., Gachon, P., Caya, D., Laprise, R., 2004. Modelling the sea ice-ocean seasonal cycle in Hudson Bay, Foxe Basin, and Hudson Strait. Canada. Clim. Dyn. 23, 303–326. https://doi.org/10.1007/s00382-004-0445-6.
Schubert, C.J., Calvert, S.E., 2001. Nitrogen and carbon isotopic composition of marine and terrestrial organic matter in Arctic Ocean sediments. Deep Sea Res. Part I

Oceanogr. Res. Pap. 48, 789–810. https://doi.org/10.1016/S0967-0637(00)00069-8.
Semiletov, I., Pipko, I., Gustafsson, Ö., Anderson, L.G., Sergienko, V., Pugach, S., Dudarev, O., Charkin, A., Gukov, A., Bröder, L., Andersson, A., Spivak, E., Shakhova, N., 2016. Acidification of East Siberian Arctic Shelf waters through addition of freshwater and terrestrial carbon. Nat. Geosci. 9, 361–365. https://doi.org/10.1038/NEGO2695.
Shadwick, E.H., Thomas, H., Chierici, M., Else, B., Fransson, A., Michel, C., Miller, L.A., Mucci, A., Niemi, A., Papakyriakou, T.N., Tremblay, J.-É., 2011. Seasonal variability of the inorganic carbon system in the Amundsen Gulf region of the southeastern Beaufort Sea. Limnol. Oceanogr. 56, 303–322. https://doi.org/10.4319/lo.2011.56.1.0303.
Shakhova, N., Semiletov, I., Salyuk, A., Yusupov, V., Kosmach, D., Gustafsson, Ö., 2010. Extensive Methane Venting to the Atmosphere from Sediments of the East Siberian Arctic Shelf. Sci. 327, 1246–1250. https://doi.org/10.1126/science.1182221.
Sibert, V., Zakardjian, B., Gosselin, M., Starr, M., Senneville, S., LeClainche, Y., 2011. 3D bio-physical model of the sympagic and planktonic productions in the Hudson Bay system. J. Mar. Syst. 88, 401–422. https://doi.org/10.1016/j.jmarsys.2011.03.014.
St-Laurent, P., Straneo, F., Dumais, J.-F., Barber, D.G., 2011. What is the fate of the river waters of Hudson Bay? J. Mar. Syst. 88, 352–361. https://doi.org/10.1016/j.jmarsys.2011.02.004.
Stedmon, C.A., Markager, S., 2001. The optics of chromophoric dissolved organic matter (CDOM) in the Greenland Sea: an algorithm for differentiation between marine and terrestrially derived organic matter. Limnol. Oceanogr. 46, 2087–2093. https://doi.org/10.4319/lo.2001.46.8.2087.
Stein, R., Macdonald, R.W., 2004a. The Organic Carbon Cycle in the Arctic Ocean. Springer, Berlin Heidelberg, Berlin, Heidelberg. https://doi.org/10.1007/978-3-642-18912-8.
Stein, R., Macdonald, R.W., 2004b. Organic carbon budget: Arctic Ocean vs. Global Ocean. In: Stein, R., MacDonald, R.W. (Eds.), The Organic Carbon Cycle in the Arctic Ocean. Springer, Berlin, Heidelberg.
Stein, R., Macdonald, R.W., Naidu, A.S., Yunker, M.B., Gobeil, C., Cooper, L.W., Grebmeier, J.M., Whitledge, T.E., Hameedi, M.J., Petrova, V.I., Batova, G.I., Zinchenko, A.G., Kursheva, A., Narkevskiy, E.V., Fahl, K., Vetrov, A., Romankevich, E.A., Birgel, D., Schubert, C., Harvey, H.R., Weiel, D., 2004. Organic carbon in arctic ocean sediments: sources, variability, burial, and paleoenvironmental significance organic carbon. In: Stein, R., MacDonald, R.W. (Eds.), The Organic Carbon Cycle in the Arctic Ocean. Springer, Berlin, Heidelberg. https://doi.org/10.1007/978-3-642-18912-8_7.
Striegl, R.G., Dornblaser, M.M., McDonald, C.P., Rover, J.R., Stets, E.G., 2012. Carbon dioxide and methane emissions from the Yukon River system. Global Biogeochem. Cycles 26. https://doi.org/10.1029/2012GB004306.
Stroeve, J., Serreze, M., 2008. Arctic sea ice extent plummets in 2007. Eos, Trans. 89, 13–14. https://doi.org/10.1029/2007GL032043.Nghiem.
Timko, S.A., Maydanov, A., Pittelli, S.L., Conte, M.H., Cooper, W.J., Koch, B.P., Schmitt-Kopplin, P., Gonsior, M., 2015. Depth-dependent photodegradation of marine dissolved organic matter. Front. Mar. Sci. 2, 1–13. https://doi.org/10.3389/fmars.2015.00066.
Vancoppenolle, M., Bopp, L., Madec, G., Dunne, J., Ilyina, T., Halloran, P.R., Steiner, N., 2013. Future arctic ocean primary productivity from CMIP5 simulations: Uncertain outcome, but consistent mechanisms. Global Biogeochem. Cycles 27, 605–619. https://doi.org/10.1002/gbc.20055.
Vonk, J.E., Sanchez-Garca, L., Van Dongen, B.E., Alling, V., Kosmach, D., Charkin, A., Semiletov, I.P., Dudarev, O.V., Shakhova, N., Roos, P., Eglinton, T.I., Andersson, A., Gustafsson, A., 2012. Activation of old carbon by erosion of coastal and subsea permafrost in Arctic Siberia. Nature 489, 137–140. https://doi.org/10.1038/nature11392.
Vonk, J.E., Tank, S.E., Bowden, W.B., Laurion, I., Vincent, W.F., Alekseychik, P., Amyot, M., Billet, M.F., Canário, J., Cory, R.M., Deshpande, B.N., Helbig, M., Jammet, M., Karlsson, J., Larouche, J., MacMillan, G., Rautio, M., Walter Anthony, K.M., Wickland, K.P., 2015. Reviews and syntheses: effects of permafrost thaw on Arctic aquatic ecosystems. Biogeosciences 12, 7129–7167. https://doi.org/10.5194/bg-12-7129-2015.
Walker, B.D., Beaupré, S.R., Guilderson, T.P., McCarthy, M.D., Druffel, E.R.M., 2016. Pacific carbon cycling constrained by organic matter size, age and composition relationships. Nat. Geosci. 9, 888–891. https://doi.org/10.1038/ngeo2830.
Welch, H.E., Bergmann, M.A., Siferd, T.D., Arnarualik, P.S., 1991. Seasonal Development of Ice Algae Near Chesterfield Inlet, N.W.T, Canada. Can. J. Fish. Aquat. Sci. 48, 2395–2402. https://doi.org/10.1139/f91-280.
Zeebe, R.E., Wolf-Gladrow, 2001. CO_2 in Seawater: Equilibrium, Kinetics, Isotopes. Elsevier Oceanography Series, 65, Amsterdam.